NAVAL POSTGRADUATE SCHOOL
Monterey, California

THESIS

A 3D THEODORSEN-BASED ROTOR BLADE FLUTTER MODEL USING NORMAL MODES

by

Werner J. Rauchenstein Jr.

September 2002

Thesis Co-Advisors: E. Roberts Wood
Mark. A. Couch

THIS PAGE INTENTIONALLY LEFT BLANK

REPORT DOCUMENTATION PAGE			Form Approved OMB No. 0704-0188
Public reporting burden for this collection of information is estimated to average 1 hour per response, including the time for reviewing instruction, searching existing data sources, gathering and maintaining the data needed, and completing and reviewing the collection of information. Send comments regarding this burden estimate or any other aspect of this collection of information, including suggestions for reducing this burden, to Washington headquarters Services, Directorate for Information Operations and Reports, 1215 Jefferson Davis Highway, Suite 1204, Arlington, VA 22202-4302, and to the Office of Management and Budget, Paperwork Reduction Project (0704-0188) Washington DC 20503.			
1. AGENCY USE ONLY *(Leave blank)*	**2. REPORT DATE** September 2002	**3. REPORT TYPE AND DATES COVERED** Master's Thesis	
4. TITLE AND SUBTITLE: **A 3D Theodorsen-based Rotor Blade Flutter Model Using Normal Modes**			**5. FUNDING NUMBERS**
6. AUTHOR(S)			
7. PERFORMING ORGANIZATION NAME(S) AND ADDRESS(ES) Naval Postgraduate School Monterey, CA 93943-5000			**8. PERFORMING ORGANIZATION REPORT NUMBER**
9. SPONSORING /MONITORING AGENCY NAME(S) AND ADDRESS(ES) N/A			**10. SPONSORING/MONITORING AGENCY REPORT NUMBER**
11. SUPPLEMENTARY NOTES The views expressed in this thesis are those of the author and do not reflect the official policy or position of the Department of Defense or the U.S. Government.			
12a. DISTRIBUTION / AVAILABILITY STATEMENT Approved for public release; distribution is unlimited			**12b. DISTRIBUTION CODE**

13. ABSTRACT ***(maximum 200 words)***

This thesis presents a fully coupled, quasi-3D analysis of rotor blade flutter that can accommodate forward flight conditions. The rotor blade is modeled as a uniform beam, taking the average characteristics of a real blade between 20% and 90% of its length. Applying Rayleigh's method, the first few bending and torsion normal mode shapes and natural frequencies are determined, and then adjusted for the rotating case. With this data, force and moment equations of motion are developed using Lagrange's equation along with a normal mode analysis. Theodorsen coefficients are calculated over a range of forward velocities (input as reduced frequencies) for a specified number of elements along the blade model. Incorporating these coefficients into the equations of motion, a square matrix is generated from which complex eigenvalues can be derived. These eigenvalues provide the aeroelastic natural frequencies and damping coefficients for each coupled mode. The forward velocity at which one of the modes produces a positive damping coefficient gives the value of reduced frequency for the flutter point. The resulting forward speed and blade tip speed can then be determined.

14. SUBJECT TERMS Rotorary Wing Structural Dynamics, Torsional Deflection, Bending Deflection, Rotor Blade Aeroelasticity, Theodorsen Lift Deficiency, Flutter Analysis, Helicopter Dynamics			**15. NUMBER OF PAGES** 75
			16. PRICE CODE
17. SECURITY CLASSIFICATION OF REPORT Unclassified	**18. SECURITY CLASSIFICATION OF THIS PAGE** Unclassified	**19. SECURITY CLASSIFICATION OF ABSTRACT** Unclassified	**20. LIMITATION OF ABSTRACT** UL

NSN 7540-01-280-5500 Standard Form 298 (Rev. 2-89)
Prescribed by ANSI Std. 239-18

THIS PAGE INTENTIONALLY LEFT BLANK

Approved for public release; distribution is unlimited

A 3D THEODORSEN-BASED ROTOR BLADE FLUTTER MODEL USING NORMAL MODES

Werner J. Rauchenstein Jr.
Lieutenant, United States Navy
B.S., United States Naval Academy, 1993

Submitted in partial fulfillment of the
requirements for the degree of

MASTER OF SCIENCE IN AERONAUTICAL ENGINEERING

from the

NAVAL POSTGRADUATE SCHOOL
September 2002

Author: Werner J. Rauchenstein Jr.

Approved by: E. Roberts Wood
Thesis Co-Advisor

Mark A. Couch
Thesis Co-Advisor

Max Platzer
Chairman, Department of Aeronautics and Astronautics

THIS PAGE INTENTIONALLY LEFT BLANK

ABSTRACT

This thesis presents a fully coupled, quasi-3D analysis of rotor blade flutter that can accommodate forward flight conditions. The rotor blade is modeled as a uniform beam, taking the average characteristics of a real blade between 20% and 90% of its length. Applying Rayleigh's method, the first few bending and torsion normal mode shapes and natural frequencies are determined, and then adjusted for the rotating case. With this data, force and moment equations of motion are developed using Lagrange's equation along with a normal mode analysis. Theodorsen coefficients are calculated over a range of forward velocities (input as reduced frequencies) for a specified number of elements along the blade model. Incorporating these coefficients into the equations of motion, a square matrix is generated from which complex eigenvalues can be derived. These eigenvalues provide the aeroelastic natural frequencies and damping coefficients for each coupled mode. The forward velocity at which one of the modes produces a positive damping coefficient gives the value of reduced frequency for the flutter point. The resulting forward speed and blade tip speed can then be determined.

THIS PAGE INTENTIONALLY LEFT BLANK

TABLE OF CONTENTS

THIS PAGE INTENTIONALLY LEFT BLANK

LIST OF FIGURES

THIS PAGE INTENTIONALLY LEFT BLANK

LIST OF TABLES

THIS PAGE INTENTIONALLY LEFT BLANK

LIST OF VARIABLES

λ – inflow ratio
ξ – non-dimensional distance from mid-chord
μ – advance ratio, $\mu=V/\Omega r$
$\varphi 1$ – phase angle between initiation of rotation input and arbitrary reference point
$\varphi 2$ – phase angle between initiation of amplitude input and arbitrary reference point
γ_a – vorticity generated by reference airfoil
γ_{nq} – vorticity generated by qth blade in nth revolution
A – aerodynamic terms in flutter equations
a – non-dimensional elastic axis location measured from mid-chord
AC – aerodynamic center
A_n – mode shape coefficients
A_n – natural frequency coefficients
b – semi-span
$C'(k,h,m)$ – Loewy's lift deficiency function
C(k) – Theodorsen's lift deficiency function
$C'_N(k,h,m)$ – finite-wake lift deficiency function
$C_1(k,\mu,\lambda)$ – Shipman-Wood lift deficiency function
CG – center of gravity
D – dissipation function
d – length of one element
DOF – degree(s) of freedom
e – flapping hinge offset from center of rotation
E – Young's Modulus
EA – elastic axis
F – real part of C(k)
F_n – edge-wise mode shape
f_n – flap-wise mode shape
g – mode damping coefficient
G – imaginary part of C(k)
GJ – torsional stiffness
H – Hankel function
h – non-dimensional distance between layers of shed vorticity (wake spacing), $h = 2\pi v/bQ\Omega$
h_n – displacement due to flapping
I_{xx} – flap-wise moment of inertia
I_α – polar mass moment of inertia
J – real Bessel function
k – reduced frequency $k=\omega b/\Omega$
K_n – Southwell coefficient
l – length of blade
L' – lift per unit span
L_h – lift due to plunge
L_α – lift due to pitch
m – mass
m – ratio of oscillation frequency to rotational frequency, $m=\omega/\Omega$
M' – moment per unit span
M_h – moment due to plunge
M_n – n^{th} mode generalized mass
M_α – moment due to pitch
n – 1, 2, 3,…
Q_n – generalized force for n^{th} mode
q_n – normal coordinate for n^{th} mode
R – blade radius
r – radial position along blade
S_α – static moment
T – kinetic energy
U – potential energy
U_{FL} – flutter velocity
U_t – blade tip velocity
V – free-stream velocity
W – Loewy's wake weighting
W_N – finite-wake weighting function
X – vector of normal coordinates
Y – imaginary Bessel function
y_n – n^{th} mode shape
Z – complex □igenvalues

α_n – displacement due to torsion
μ – mass per unit length
ρ – density of air
ψ – blade azimuth position
ω – frequency of oscillation
Ω – rotor velocity

ACKNOWLEDGMENTS

I would like to thank the following people who were critical to my successfully completing this thesis. Dr. E. R. Wood suggested the topic, served as co-advisor, assisted me throughout the research process, and provided extensive insight into every aspect of this work, as well as many insights not included in this work. CDR M. A. Couch served as co-advisor and provided a significant amount of time, energy and grass-roots explanations of vastly complex phenomena. Mr. Robert Goodman at Sikorsky Aircraft Company coordinated for the authorized release of data pertaining to their natural frequency calculations. Dr. Max Platzer and Dr. Hobson shared with me their enthusiasm for unsteady aerodynamics and their desire for a physical and intuitive understanding of this type of phenomena. Finally, and most importantly, my wife gave me the support, confidence and understanding so necessary during the last year.

THIS PAGE INTENTIONALLY LEFT BLANK

I. INTRODUCTION

A. INTRODUCTION

The conventional method for designing a rotor blade to be free of flutter throughout the helicopter's flight regime is to design the blade so that aerodynamic center (AC), elastic axis (EA) and center of gravity (CG) are coincident and located at the quarter-chord. This practice pays off by decoupling the equations used in two-dimensional unsteady aerodynamic theory. While this assures freedom from flutter, it adds constraints on rotor blade design not usually followed in fixed wing design. A blade designed with the CG, EA and AC coincident at the quarter chord is heavier than one free of that restriction. It also, if strictly followed, rules out use of a flap that causes the AC to move with flap angle. In addition, it restricts use of camber that moves the AC aft [Ref. 1].

Loewy's [Ref. 2] 2-D unsteady aerodynamic theory, as amended by Jones and Rao [Ref. 3] and Hammond [Ref. 4], provides a useful tool for examining blade flutter in a hover. Extension of their work to a helicopter in forward flight presents a formidable mathematical challenge, and thus, at present, there is no accepted theory to completely analyze blade flutter in forward flight. Currently, to meet forward flight blade flutter requirements the rotorcraft manufacturer must rely on: (1) a quasi-fixed wing blade flutter analysis, which does not account for the unsteady contribution of the wake below the rotor; and (2) costly rotor whirl tests at normal and over-speed conditions that, while providing information in regard to blade flutter, do not accurately simulate either blade dynamics or unsteady aerodynamics in forward flight.

However, closer examination of the problem reveals that it is possible to make several simplifying assumptions that make the forward flight flutter problem tractable. In particular, it is assumed that at the onset of flutter oscillations begin to build up prior to the blade reaching a critical azimuth position, then decay as the blade moves beyond this point. Shipman and Wood [Ref. 5] provide the two-dimensional basis for this three-dimensional analysis. This thesis will follow the analysis of Shipman and Wood, using Theodorsen's lift deficiency function (2-D approach), and further expand the theory to

encompass full blade-length dynamics (3-D effects). A numerical example using UH-60 blade data is included as a means of illustration and validation.

B. BACKGROUND

> *"Main and tail rotor blades of the A.T.H. have been designed so that center of gravity, elastic axis, and aerodynamic center are coincident. Also, the control system for the main rotor is stiff with high internal damping. No main or tail rotor blade flutter has been experienced with earlier model helicopters possessing these design features.*
>
> *Main and tail rotor blades for the HSS-2, which are the same as those of the A.T.H., have been installed on Sikorsky whirl stands, and tested at maximum design-limit speeds. Main rotor blades were tested for power-on and power-off conditions. Tail rotor test conditions were power-on and power-off. Observation of blades during these tests indicated no flutter or divergence at maximum operating conditions."* [Ref. 6]

This statement, from the 1960 Sikorsky Report No. 50131 for the Advanced Tactical Helicopter, is representative of the current methods for ascertaining freedom from flutter for new helicopter acquisitions. Theoretical calculations consist of a 2-D flutter analysis of the blade tip as if it was a fixed wing, and whirl stand tests involve significant expense. Much effort has been expended in the last century to improve flutter prediction and minimize the cost in time and money spent on whirl stand tests. The following paragraphs are a review of some of the significant work that has advanced the study of flutter and provided methods of solving the flutter problem.

1. Theodorsen and Loewy

In 1936, Theodorsen [Ref. 7] made the flutter problem somewhat tractable with certain simplifying assumptions. He considered a wing of infinite aspect ratio, encountering small oscillations at a constant velocity through an incompressible, non-viscous fluid. By using these assumptions, the forces and moments could be determined from 2-D potential flow theory. In addition, instead of using the actual mass and geometry distributions, he assumed that the results could be conservatively obtained for a unit span of the wing. Using the nomenclature found in Scanlan and Rosenbaum [Ref. 8], and excluding terms associated with an aileron, the unsteady force and moment per unit span are given by

$$L' = \pi\rho b^3\omega^2\left\{L_h\frac{h}{b} + \left[L_\alpha - \left(\frac{1}{2}+a\right)L_h\right]\alpha\right\}$$

and

$$M' = \pi\rho b^4\omega^2\left\{\left[M_h - \left(\frac{1}{2}+a\right)L_h\right]\frac{h}{b} + \left[M_\alpha - \left(\frac{1}{2}+a\right)\left(L_\alpha + M_h\right) + \left(\frac{1}{2}+a\right)^2 L_h\right]\alpha\right\}$$

where

$$L_h = 1 - \frac{2i}{k}C(k)$$

$$L_\alpha = \frac{1}{2} - \frac{2i}{k}\left[\frac{1}{2} + \left(1 - \frac{i}{k}\right)C(k)\right]$$

$$M_h = \frac{1}{2}$$

$$M_\alpha = \frac{3}{8} - \frac{i}{k}$$

The term $C(k)$ is Theodorsen's well-known lift deficiency function defined by

$$C(k) = \frac{H_1^{(2)}}{H_1^{(2)} + iH_0^{(2)}}$$

where $H_n^{(2)} = J_n - iY_n$ is the Hankel function of the second kind of order n evaluated at reduced frequency k = ωb/V. The force and moment equations take into account both pitch (torsion) and plunge (flapping) motion, and include circulatory and non-circulatory terms. It is in the circulatory terms that the lift deficiency function is defined.

Inherent in Theodorsen's 2-D thin airfoil theory is the assumption that the wake is carried downstream to infinity by the free-stream airflow [Ref. 9]. For work in rotor blade flutter, this assumption presents problems, since the rotor blade sections may encounter the shed wake from previous blades as well as the reference airfoil. Loewy [Ref. 2] recognized this problem and developed a 2-D model for the hover case that accounted for the effects of previously shed wakes. The wakes were modeled as a series

of planar 2-D vortex sheets separated by a distance 'h' that was dependent on the induced velocity through the rotor disk and the number of rotor blades. Loewy then developed a modified lift deficiency function that could be used in conjunction with the force and moment equations. This modified lift deficiency function is defined as

$$C'(k,m,h) = \frac{H_1^{(2)}(k) + 2J_1(k)W(k,m,h)}{H_1^{(2)}(k) + iH_0^{(2)}(k) + 2[J_1(k) + iJ_0(k)]W(k,m,h)}$$

where

$$W(k,m,h) = \frac{1}{e^{\frac{kh}{b}} e^{i2\pi(m)} - 1}$$

and is evaluated at reduced frequency (k), wake spacing ($h = 2\pi V/bQ\Omega$) and frequency ratio ($m = \omega/\Omega$). Note that as $h \to \infty$, $W \to 0$ and $C'(k) \to C(k)$.

2. Shipman and Wood

In 1971, Shipman and Wood [Ref. 5] examined the unsteady aerodynamics acting on an advancing blade in steady-state level flight. The basic assumptions of their work are as follows:

1. Two-dimensional, inviscid, incompressible potential flow.
2. Respective layers of the wake are two-dimensionalized and treated as parallel horizontal sheets.
3. In forward flight, each blade of the rotor will respond in the same manner as every other blade.
4. The most critical azimuth position of the blade in forward flight for the onset of flutter is at $\psi = 90^{\circ}$.
5. At the onset of blade flutter, oscillations will begin to build up prior to the blade reaching the critical azimuth position, and these oscillations will decay as the blade moves beyond the critical azimuth position.

At a specified radial location r on the blade, the local tangential velocity is given by

$$U_t(r) = \Omega r + V \sin\psi$$

If it is assumed that the flutter speed for this blade segment is such that

$$U_{FL}(r) < \Omega r + V$$

then during each blade revolution the blade segment at radius 'r' will experience velocities which will increase to the flutter speed and beyond, then return through the flutter point to lower airspeeds. Extending this concept to both blade azimuth position and radial position, one can observe that the blade tangential velocity at a given radial position will exceed the flutter speed in some region of rotor azimuth position if:

$$V \sin \psi > U_{FL}(r) - \Omega r$$

This flutter region is illustrated in Fig. 1.

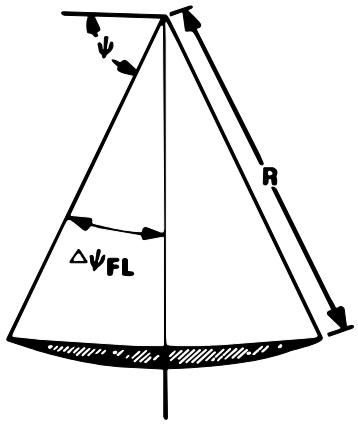

Figure 1. Unstable Region on Advancing Blade

It should be noted that all points within the shaded region of Fig. 1 experience negative damping. This negative damping when combined with transient oscillations in the blade and will cause blade motion to grow. Also, in the region $\psi \leq \pi/2 - \Delta\psi_{FL}$, the damping will decrease as ψ approaches $(\pi/2 - \Delta\psi_{FL})$, whereas in the region $\psi \geq \pi/2 + \Delta\psi_{FL}$, damping will be positive and will increase such that blade transients tend to die out.

Consider the effect of this variation in damping on an outboard portion of the advancing blade. It is expected that damping would decrease as the blade approaches $\psi = 90^{\circ}$ and the amplitude of oscillations would build up. Conversely, as the blade advanced beyond $\psi = 90^{\circ}$, damping would increase, and there would be a corresponding decrease in blade vibratory amplitude. This build-up and decay of blade amplitude would result in a distribution of shed vorticity as shown by Fig. 2. Here, we observe that time-wise variations in amplitude of blade vibrations have resulted in space-wise variations in

shed vorticity. Since we have assumed steady-state flight, each blade would shed similar segments of vorticity for each revolution. These vortex segments constitute the wake that will be treated in this analysis.

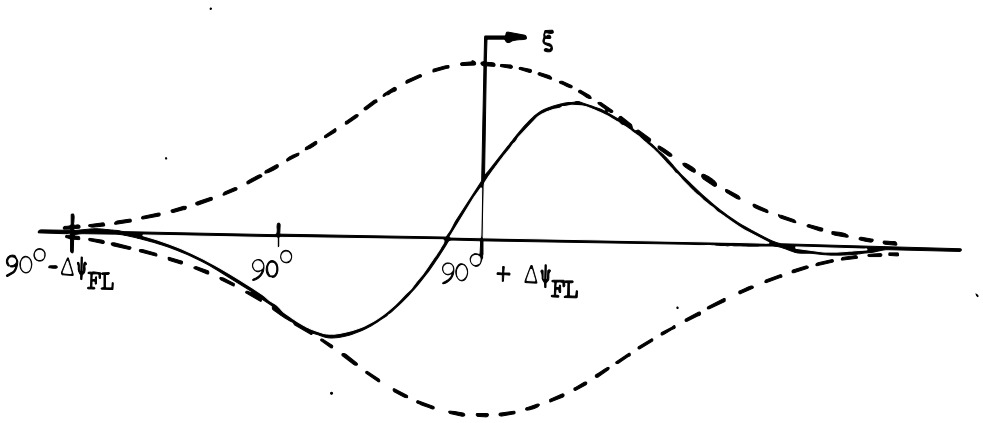

Figure 2. Distribution of Shed Vorticity in Unstable Region

Based on the foregoing, the bound vorticity on the airfoil can be expressed as the product of a function of chord-wise position, a decay function, and a harmonic function of time[1]. We write the incremental bound vorticity as

$$\gamma_a = \bar{\gamma}_a(x) f(\xi_0) e^{i(\omega t + \phi)}$$

where $f(\xi_0)$ is an assumed decay function centered about $\xi_0 = 0$. The limiting case of constant-strength shed vorticity such as considered by Theodorsen [Ref. 7] and Loewy [Ref. 1] for their analyses, is simply achieved by taking $f(\xi_0) = 1$.

When the inflow velocity through the rotor is small, the shed vorticity remains close to the rotor and the wakes shed from each blade during several previous passes as well as the present pass must be considered. The build-up and decay of vorticity occurs within a double azimuth angle on either side of $\psi = 90^\circ$. The solid lines of Fig. 3 indicate this region of the wake. In this region the azimuth angle between a shed vortex filament and the reference blade may be ignored. The tip does not move very far from the vertical plane shown in Fig. 3 and so its path may be taken to lie in this plane.

[1] W. P. Jones [Ref. 10] first treated the case of an oscillating airfoil where the strength of the airfoil's position was allowed to grow or decay exponentially with time. As the buildup or decay rate approached zero, Jones' lift deficiency function approached that of Theodorsen [Ref. 6].

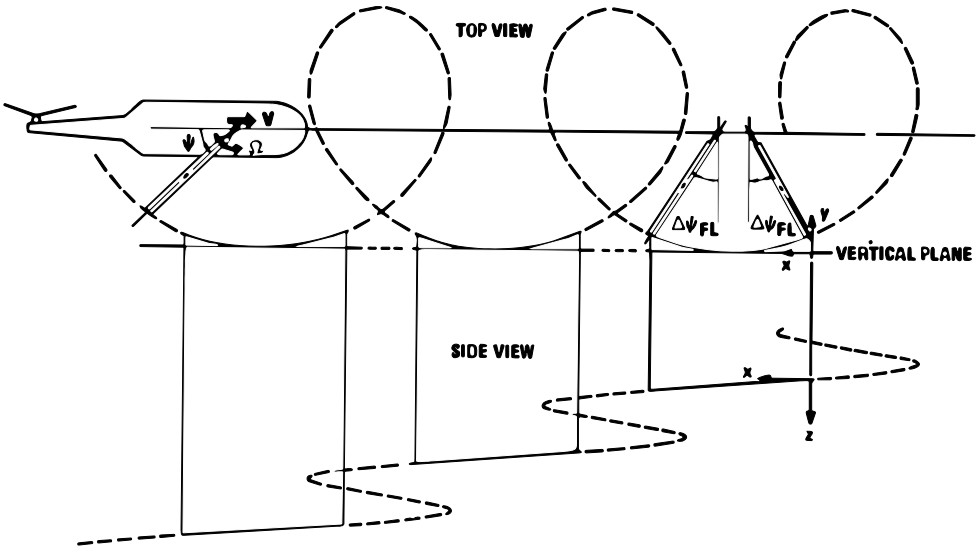

Figure 3. Development of Skewed Helical Wake

Combining the vorticity segments given in Fig. 2, the resulting wake pattern is shown in Fig. 4. With the mathematical model defined, the problem now is to determine the pressure difference across the airfoil due to the vorticity shed in the wake, and consequently to determine the unsteady lift and moment acting on the airfoil.

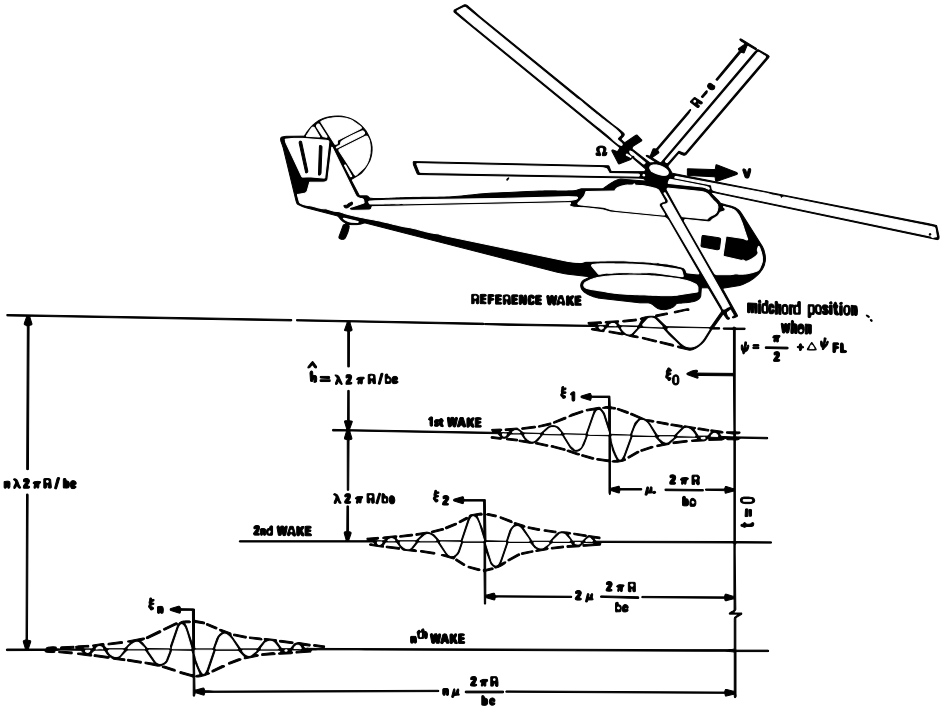

Figure 4. 2-D Wake Model for Forward Flight

Shipman and Wood developed their equation for the unsteady forces in forward flight that are analogous to Theodorsen and Loewy, but modified the lift deficiency function to account for the helicopter's forward speed (advance ratio) and the build-up and decay function associated with the advancing blade illustrated in Fig. 2. The forward flight lift deficiency function is defined by

$$C_1(k,h,m) = \frac{H_1^{(2)}(k) + \Delta F_2(k) + \Delta F_4(k) + 2J_1(k) \;\; \left[W(k,h,m) + \Delta W(k,h,m)\right]}{H_1^{(2)}(k) + iH_0^{(2)}(k) + \Delta F_3(k) + 2\left(J_1(k) + iJ_0(k)\right) \;\; \left[W(k,h,m) + \Delta W(k,h,m)\right]}$$

where

$$\Delta F_2(k) = -\frac{2}{\pi}\int_1^\infty \left[f(y) - 1 - \frac{1}{ik}\frac{df}{dy}\right]\frac{ye^{-iky}}{\sqrt{y^2-1}}\,dy$$

$$\Delta F_3(k) = -\frac{2}{\pi}\int_1^\infty \left[f(y) - 1 - \frac{1}{ik}\frac{df}{dy}\right]\left(\sqrt{\frac{y+1}{y-1}}\right)e^{-iky}\,dy$$

$$\Delta F_4(k) = -\frac{2}{\pi}\int_1^\infty \left[\frac{df}{dy} - \frac{1}{ik}\frac{d^2f}{dy^2}\right]\left[y - \sqrt{y^2-1}\right]e^{-iky}\,dy$$

$$\Delta W(k,h,m) = \sum_{n=1}^{\infty} e^{-knh}e^{iknm} \times \left[f(-nm-inh) - 1 - \frac{1}{ik}\frac{df(-nm-inh)}{dy}\right]$$

where f(y) is the assumed decay function. Note that as $h \to \infty$, and $s \to \infty$, $C_1(k) \to C(k)$, and when $V \to 0$, $C_1(k) \to C'(k)$.

II. THEORETICAL DEVELOPMENT

A. A FLUTTER THEORY FOR FORWARD FLIGHT

Shipman and Wood, using the theory described in the previous section derived an equation analogous to Theodorsen and Loewy that accounted for the effects of forward flight and a shed skewed helical wake. However, evaluation of some of the integrals required for the ΔF and ΔW terms is extremely difficult. If the view is taken that the Theodorsen method, which neglects the effect of the shed wakes, is just a first-order approximation to the rotary-wing flutter problem, then use of the Theodorsen lift deficiency function should yield suitable first-order results. Therefore, this thesis will rely on Theodorsen's lift deficiency function, while following the methods of Shipman and Wood in modeling forward flight.

1. Mode Shapes and Natural Frequencies

Blade bending frequencies and mode shapes used in this analysis were determined by a simplified method by assuming a uniform stiffness and mass distribution along the blade. A more exact and detailed analysis would be required to account for such details such as local changes in stiffness and mass distribution due to blade features such as doublers near the blade root and outboard blade balance weights near the tip. While these details would be desired for an actual blade design, they can be viewed as second order effects and not necessary for the first order flutter analysis.

For the simplified model, the geometric and inertial properties of the subject blade are averaged between 20% and 90% of its length. The Fourier-based solution of the pinned-free uniform beam from Young and Felgar [Ref. 11] are applied to determine the non-rotating mode shapes:

$$y_n = \frac{1}{2}\left(\cosh(r) + \cos(r) - A_n\left(\sinh(r) + \sin(r)\right)\right)$$

where A_n = 1.000777, 1.000001 and 1.0 for the first three bending modes. Then the method given by Den Hartog [Ref. 12] for determining non-rotating natural frequencies is applied:

$$\omega_n = a_n \sqrt{\frac{EI_{xx}}{\mu R^4}}$$

where a_n = 15.4182, 49.9649 and 104.2477 for the first three bending modes, and μ is the mass per unit length.

Given the natural frequencies, the rotational velocity of the rotor head, and the non-rotating mode shapes, Yntema [Ref. 13] is called on to supply the rotating natural frequencies. Figures 5 through 7, taken from Yntema's report, compares rotating and non-rotating mode shapes for the first three bending modes of a pinned-free beam to validate the assumption that the non-rotating mode shape is a close approximation of the rotating mode shape.

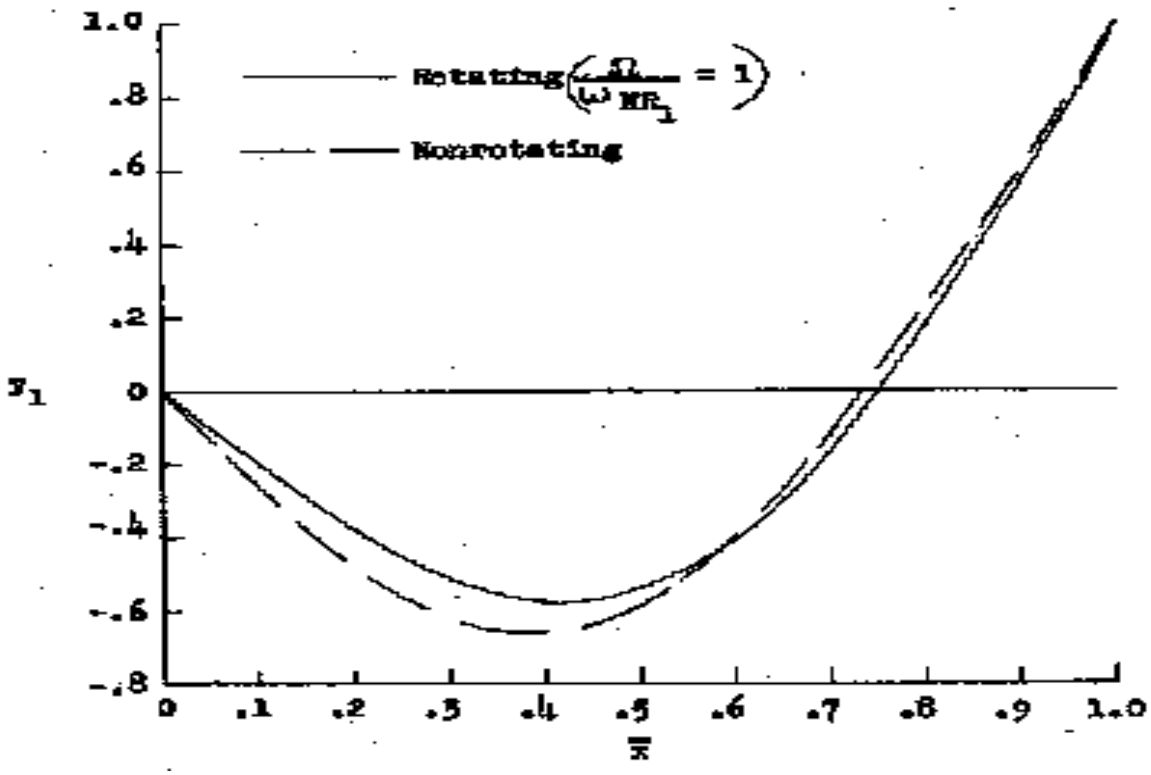

Figure 5. Rotating and Non-Rotating Mode shapes for the First Bending Mode

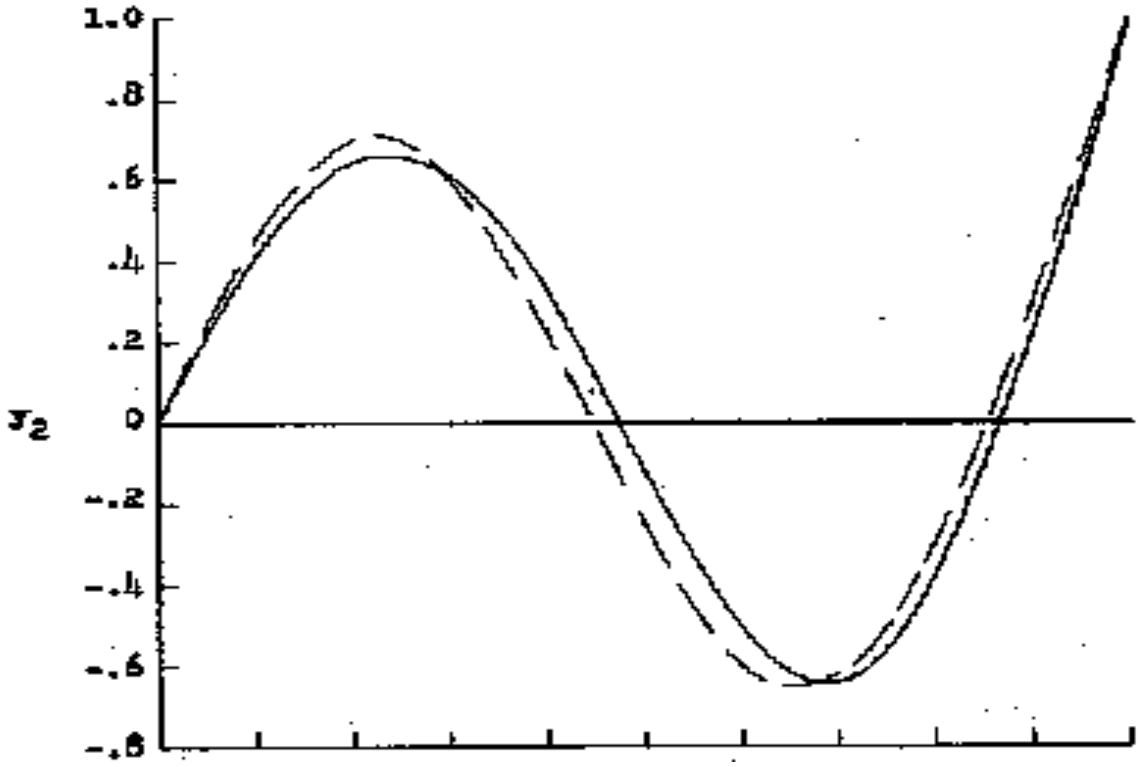

Figure 6. Rotating and Non-Rotating Mode shapes for the Second Bending Mode

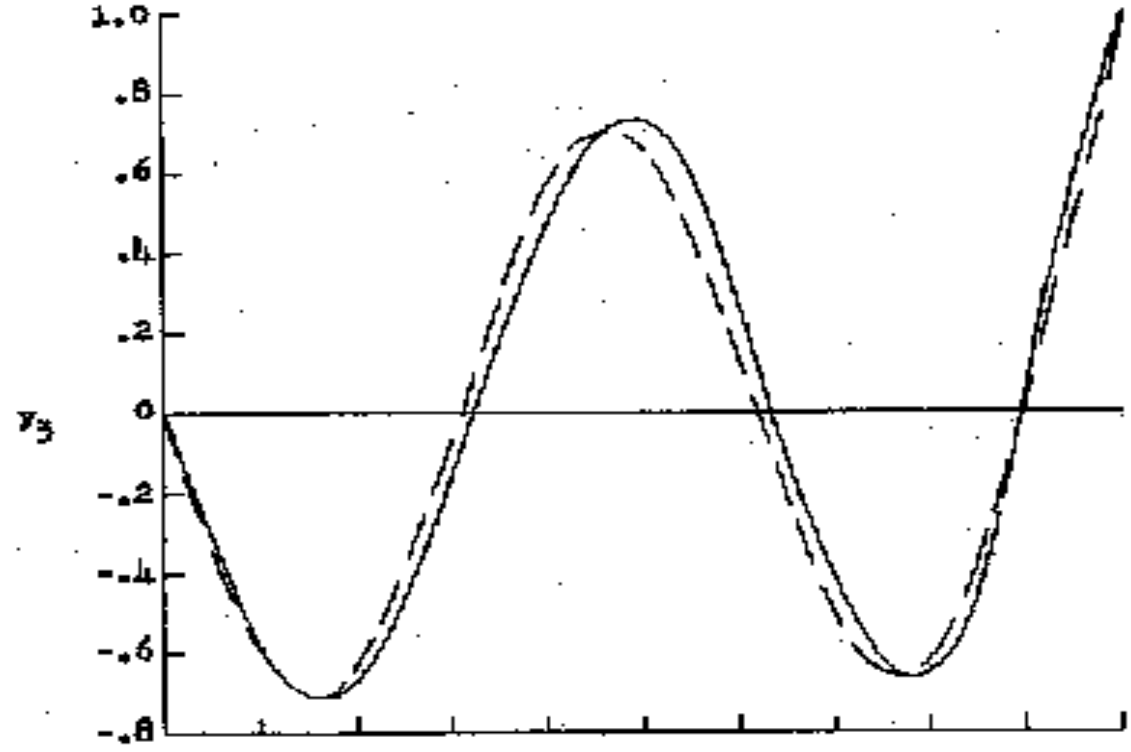

Figure 7. Rotating and Non-Rotating Mode Shapes for the Third Bending Mode

Yntema notes that an exact value for the n^{th} bending frequency of a beam rotating at any rotational speed, Ω, can be found if the n^{th} natural bending mode shape is known for this value of rotational speed. He obtains his frequency equation by equating the kinetic energy at zero displacement to the potential energy of both the bending and centrifugal forces at maximum displacement for vibration perpendicular to the plane of rotation.

$$\omega_{R_n}^2 = \frac{\int_0^l EIy_n''^2 \quad dx}{\int_0^l my_n^2 \quad dx} + \frac{\int_0^l T_l y_n'^2 \quad dx}{\int_0^l my_n^2 \quad dx} \tag{1}$$

where n refers to mode of vibration and

$$T_l = \int_x^l (\eta + e) m \quad d\eta$$

He goes on to point out that while the rotating mode shape is unknown, a close approximation to the rotating natural frequency can be obtained by making use of *Rayleigh's Principle,* and using the non-rotating mode shape in equation (1). The report states that the non-rotating mode shape is consistent with the constraints of the system (in this case a pinned-free beam). If the n^{th} mode of the non-rotating mode shape, y_n, is substituted into equation (1), the first term becomes exactly the square of the bending frequency of the non-rotating beam. By denoting the ratio in the second term by K_n, a Southwell coefficient, the form of the frequency equation becomes:

$$\omega_{R_n}^2 = \omega_{NR_n}^2 + K_n \Omega^2 \tag{2}$$

To account for blade offset, e, subdivide K_n into two independent parts:

$$K_n = K_{0_n} + K_{1_n} e \tag{3}$$

where K_{0n} is referred to as the zero-offset Southwell coefficient and K_{1n} is referred to as the offset-correction factor for the Southwell coefficient. As is frequently done, it is convenient to write the square of the non-rotating frequency in terms of a non-rotating-beam frequency coefficient, a_n, and the mass and stiffness of the beam as:

$$\omega_{NR_n}^2 = a_n^2 \frac{EI_0}{m_0 l^4} \tag{4}$$

Combining equations (2), (3) and (4) yield:

$$\omega_{R_n}^2 = \omega_{NR_n}^2 + \left(K_{0_n} + K_{1_n} e\right)\Omega^2$$

Yntema's report [Ref. 13] gives charts that provide a_n, K_{0n} and K_{1n} which, in conjunction with the mass and stiffness of the beam at the root, the length of the beam, the hinge offset, and the rotational speed, permit rapid estimation of the first three bending frequencies of rotating beams with hinged or cantilevered root-end support. As previously noted, once the frequencies have been found, the rotating beam mode shapes can then be approximated by non-rotating mode shapes which are defined by the Fourier-based solutions contained in Young and Felgar [Ref. 11].

The next problem is to determine the mode shapes and frequencies for the uniform beam blade model in the torsional case. For this, Den Hartog [Ref. 13] provides a relatively simple solution. Given that the torsional stiffness along the beam is constant, the torsional mode shapes are given by

$$y_n = \sin\left(\frac{\left(n - \frac{1}{2}\right)\pi r}{R}\right)$$

The non-rotating torsional natural frequencies are given by

$$\omega_{NRn} = \left(n - \frac{1}{2}\right)\pi\sqrt{\frac{GJ}{I_\alpha' R^2}}$$

Bramwell [Ref. 14], gives the exact solution for rotating natural frequencies in the torsional case as

$$\omega_{R_n}^2 = \omega_{NR_n}^2 + \Omega^2$$

2. Normal Mode Analysis

With the rotor blade free vibration problem solved, the bending deflection may be defined as

$$h(x,t) = \sum_{n=1}^{N} f_n(x) q_n(t)$$

where $f_n(x)$ is the characteristic function (mode shape) for the n^{th} vertical bending mode of the rotor blade. The quantities $q_n(t)$ can be considered as weighting functions for each mode that contributes to the deflection. They are called the normal coordinates since they can be shown to reduce the kinetic and potential energy expressions to sums of squares of the coordinates with no cross product terms.

The corresponding torsional deflection of the rotor blade can be written in terms of the blade torsion modes as:

$$\alpha(x,t) = \sum_{n=1}^{N} F_n(x) q_n(t)$$

where $F_n(x)$ is the characteristic function of the n^{th} torsional mode of the rotor blade and $q_n(t)$ is the corresponding normal coordinate. Consider the five-degree of freedom (DOF) case with three bending modes and two torsion modes. The bending and torsional deflections can be written as:

$$h(x,t) = h_1(t) f_1(x) + h_2(t) f_2(x) + h_3(t) f_3(x)$$

and

$$\alpha(x,t) = \alpha_1(t) F_1(x) + \alpha_2(t) F_2(x)$$

where

$f_1(x) = 1^{st}$ vertical bending mode
$f_2(x) = 2^{nd}$ vertical bending mode
$f_3(x) = 3^{rd}$ vertical bending mode
$F_1(x) = 1^{st}$ torsion mode
$F_2(x) = 2^{nd}$ torsion mode

Now all the tools are in place to begin the detailed flutter analysis, which is the combination of Lagrange's equation with Theodorsen's work to provide the equations of motion.

3. Lagrange and The Equations of Motion

Lagrange's equation is given as:

$$\frac{d}{dt}\left(\frac{\partial T}{\partial \dot{q}_n}\right) - \frac{\partial T}{\partial q_n} + \frac{\partial U}{\partial q_n} + \frac{\partial D}{\partial \dot{q}_n} = Q_n$$

where T ≡ kinetic energy, U ≡ potential energy, D ≡ dissipation function, and Q_n ≡ generalized force. For the five DOF case,

$$\begin{aligned} T = {} & \frac{1}{2}M_1\dot{h}_1^2 + \frac{1}{2}M_2\dot{h}_2^2 + \frac{1}{2}M_3\dot{h}_3^2 + \frac{1}{2}I_{\alpha_1}\dot{\alpha}_1^2 + \frac{1}{2}I_{\alpha_2}\dot{\alpha}_2^2 \\ & + S_{\alpha_{11}}\dot{h}_1\dot{\alpha}_1 + S_{\alpha_{12}}\dot{h}_1\dot{\alpha}_2 + S_{\alpha_{21}}\dot{h}_2\dot{\alpha}_1 \\ & + S_{\alpha_{22}}\dot{h}_2\dot{\alpha}_2 + S_{\alpha_{31}}\dot{h}_3\dot{\alpha}_1 + S_{\alpha_{32}}\dot{h}_3\dot{\alpha}_2 \end{aligned}$$

$$\begin{aligned} U = {} & \frac{1}{2}M_1\omega_{h_1}^2 h_1^2 + \frac{1}{2}M_2\omega_{h_2}^2 h_2^2 + \frac{1}{2}M_3\omega_{h_3}^2 h_3^2 \\ & + \frac{1}{2}I_{\alpha_1}\omega_{\alpha_1}^2\alpha_1^2 + \frac{1}{2}I_{\alpha_2}\omega_{\alpha_2}^2\alpha_2^2 \end{aligned}$$

$$\begin{aligned} D = {} & \frac{M_1 g_{h_1}\omega_{h_1}^2\dot{h}_1^2}{2\omega} + \frac{M_2 g_{h_2}\omega_{h_2}^2\dot{h}_2^2}{2\omega} + \frac{M_3 g_{h_3}\omega_{h_3}^2\dot{h}_3^2}{2\omega} \\ & + \frac{I_{\alpha_1} g_{\alpha_1}\omega_{\alpha_1}^2\dot{\alpha}_1^2}{2\omega} + \frac{I_{\alpha_2} g_{\alpha_2}\omega_{\alpha_2}^2\dot{\alpha}_2^2}{2\omega} \end{aligned}$$

and the generalized forces including aerodynamic terms are defined as:

$$\begin{aligned} Q_{h_1} &= \pi\rho\omega^2\left(A_{11}h_1 + A_{12}h_2 + A_{13}h_3 + A_{14}\alpha_1 + A_{15}\alpha_2\right) \\ Q_{h_2} &= \pi\rho\omega^2\left(A_{21}h_1 + A_{22}h_2 + A_{23}h_3 + A_{24}\alpha_1 + A_{25}\alpha_2\right) \\ Q_{h_3} &= \pi\rho\omega^2\left(A_{31}h_1 + A_{32}h_2 + A_{33}h_3 + A_{34}\alpha_1 + A_{35}\alpha_2\right) \\ Q_{\alpha_1} &= \pi\rho\omega^2\left(A_{41}h_1 + A_{42}h_2 + A_{43}h_3 + A_{44}\alpha_1 + A_{45}\alpha_2\right) \\ Q_{\alpha_2} &= \pi\rho\omega^2\left(A_{51}h_1 + A_{52}h_2 + A_{53}h_3 + A_{54}\alpha_1 + A_{55}\alpha_2\right) \end{aligned}$$

The expressions for aerodynamic terms that couple the modes together and incorporate Theodorsen's lift deficiency function are given as

$$A_{11} = \int_0^1 b^2 \left[f_1(x) \right]^2 L_h dx \tag{5}$$

$$A_{12} = \int_0^1 b^2 f_1(x) f_2(x) L_h dx$$

$$A_{13} = \int_0^1 b^2 f_1(x) f_3(x) L_h dx$$

$$A_{14} = \int_0^1 b^3 f_1(x) F_1(x) \left[L_\alpha - \left(\frac{1}{2} + a \right) L_h \right] dx$$

$$A_{15} = \int_0^1 b^3 f_1(x) F_2(x) \left[L_\alpha - \left(\frac{1}{2} + a \right) L_h \right] dx$$

$$A_{21} = \int_0^1 b^2 f_2(x) f_1(x) L_h dx = A_{12}$$

$$A_{22} = \int_0^1 b^2 \left[f_2(x) \right]^2 L_h dx$$

$$A_{23} = \int_0^1 b^2 f_2(x) f_3(x) L_h dx$$

$$A_{24} = \int_0^1 b^3 f_2(x) F_1(x) \left[L_\alpha - \left(\frac{1}{2} + a \right) L_h \right] dx$$

$$A_{25} = \int_0^1 b^3 f_2(x) F_2(x) \left[L_\alpha - \left(\frac{1}{2} + a \right) L_h \right] dx$$

$$A_{31} = \int_0^1 b^2 f_3(x) f_1(x) L_h dx = A_{13}$$

$$A_{32} = \int_0^1 b^2 f_3(x) f_2(x) L_h dx = A_{23}$$

$$A_{33} = \int_0^1 b^2 \left[f_3(x) \right]^2 L_h dx$$

$$A_{34} = \int_0^1 b^3 f_3(x) F_1(x) \left[L_\alpha - \left(\frac{1}{2} + a \right) L_h \right] dx$$

$$A_{35} = \int_0^1 b^3 f_3(x) F_2(x) \left[L_\alpha - \left(\frac{1}{2} + a \right) L_h \right] dx$$

$$A_{41} = \int_0^1 b^3 F_1(x) f_1(x) \left[M_h - \left(\frac{1}{2} + a \right) L_h \right] dx$$

$$A_{42} = \int_0^1 b^3 F_1(x) f_2(x) \left[M_h - \left(\frac{1}{2} + a \right) L_h \right] dx$$

$$A_{43} = \int_0^1 b^3 F_1(x) f_3(x) \left[M_h - \left(\frac{1}{2} + a \right) L_h \right] dx$$

$$A_{44} = \int_0^1 b^4 \left[F_1(x) \right]^2 \left[M_\alpha - \left(\frac{1}{2} + a \right) (L_\alpha + M_h) + \left(\frac{1}{2} + a \right)^2 L_h \right] dx$$

$$A_{45} = \int_0^1 b^4 F_1(x) F_2(x) \left[M_\alpha - \left(\frac{1}{2} + a \right) (L_\alpha + M_h) + \left(\frac{1}{2} + a \right)^2 L_h \right] dx$$

$$A_{51} = \int_0^1 b^3 F_2(x) f_1(x) \left[M_h - \left(\frac{1}{2} + a \right) L_h \right] dx$$

$$A_{52} = \int_0^1 b^3 F_2(x) f_2(x) \left[M_h - \left(\frac{1}{2} + a \right) L_h \right] dx$$

$$A_{53} = \int_0^1 b^3 F_2(x) f_3(x) \left[M_h - \left(\frac{1}{2} + a \right) L_h \right] dx$$

$$A_{54} = \int_0^1 b^4 F_2(x) F_1(x) \left[M_\alpha - \left(\frac{1}{2} + a \right) (L_\alpha + M_h) + \left(\frac{1}{2} + a \right)^2 L_h \right] dx = A_{45}$$

$$A_{55} = \int_0^1 b^4 \left[F_2(x) \right]^2 \left[M_\alpha - \left(\frac{1}{2} + a \right) \ (L_\alpha + M_h) + \left(\frac{1}{2} + a \right)^2 L_h \right] dx$$

The generalized masses of the three bending modes and two torsion modes can be written as:

$$M_1 = \int_0^1 m(x) \left[f_1(x) \right]^2 dx$$

$$M_2 = \int_0^1 m(x) \left[f_2(x) \right]^2 dx$$

$$M_3 = \int_0^1 m(x) \left[f_3(x) \right]^2 dx$$

$$I_{\alpha_1} = \int_0^1 I_\alpha(x)\left[F_1(x)\right]^2 dx$$

$$I_{\alpha_2} = \int_0^1 I_\alpha(x)\left[F_2(x)\right]^2 dx$$

The coupled static unbalance terms are defined as:

$$S_{\alpha_{11}} = \int_0^1 S_\alpha(x) f_1(x) F_1(x) dx$$

$$S_{\alpha_{12}} = \int_0^1 S_\alpha(x) f_1(x) F_2(x) dx$$

$$S_{\alpha_{21}} = \int_0^1 S_\alpha(x) f_2(x) F_1(x) dx$$

$$S_{\alpha_{22}} = \int_0^1 S_\alpha(x) f_2(x) F_2(x) dx$$

$$S_{\alpha_{31}} = \int_0^1 S_\alpha(x) f_3(x) F_1(x) dx$$

$$S_{\alpha_{32}} = \int_0^1 S_\alpha(x) f_3(x) F_2(x) dx$$

First it is noted that the kinetic energy equation is only a function of the derivative of the generalized displacement ($\dot{h}_n$ or $\dot{\alpha}_n$). Thus, Lagrange's equation reduces to:

$$\frac{d}{dt}\left(\frac{\partial T}{\partial \dot{q}_n}\right) + \frac{\partial U}{\partial q_n} + \frac{\partial D}{\partial \dot{q}_n} = Q_n$$

Applying Lagrange's equation to each of the five DOFs yields the following five equations:

$$M_1\ddot{h}_1 + S_{\alpha_{11}}\ddot{\alpha}_1 + S_{\alpha_{12}}\ddot{\alpha}_2 + M_1\omega_{h_1}^2 h_1 + \frac{M_1\omega_{h_1}^2 g_{h_1}}{\omega}\dot{h}_1 = Q_{h_1}$$

$$M_2\ddot{h}_2 + S_{\alpha_{21}}\ddot{\alpha}_1 + S_{\alpha_{22}}\ddot{\alpha}_2 + M_2\omega_{h_2}^2 h_2 + \frac{M_2\omega_{h_2}^2 g_{h_2}}{\omega}\dot{h}_2 = Q_{h_2}$$

$$M_3\ddot{h}_3 + S_{\alpha_{31}}\ddot{\alpha}_1 + S_{\alpha_{32}}\ddot{\alpha}_2 + M_3\omega_{h_3}^2 h_3 + \frac{M_3\omega_{h_3}^2 g_{h_3}}{\omega}\dot{h}_3 = Q_{h_3}$$

$$I_{\alpha_1}\ddot{\alpha}_1 + S_{\alpha_{11}}\ddot{h}_1 + S_{\alpha_{21}}\ddot{h}_2 + S_{\alpha_{31}}\ddot{h}_3 + I_{\alpha_1}\omega_{\alpha_1}^2\alpha_1 + \frac{I_{\alpha_1}\omega_{\alpha_1}^2 g_{\alpha_1}}{\omega}\dot{\alpha}_1 = Q_{\alpha_1}$$

$$I_{\alpha_2}\ddot{\alpha}_2 + S_{\alpha_{12}}\ddot{h}_1 + S_{\alpha_{22}}\ddot{h}_2 + S_{\alpha_{32}}\ddot{h}_3 + I_{\alpha_2}\omega_{\alpha_2}^2\alpha_2 + \frac{I_{\alpha_2}\omega_{\alpha_2}^2 g_{\alpha_2}}{\omega}\dot{\alpha}_2 = Q_{\alpha_2}$$

If simple harmonic motion is assumed, that is: $\ddot{h}_n = -\omega^2 h_n$, $\dot{h}_n = i\omega h_n$, $\ddot{\alpha}_n = -\omega^2\alpha_n$, and $\dot{\alpha}_n = i\omega\alpha_n$, and the expressions for Q_{h_n} and Q_{α_n} are substituted into the equations of motion, the results are:

$$\left[\pi\rho A_{11} + M_1 - M_1\left(1 + ig_{h_1}\right)\left(\frac{\omega_{h_1}}{\omega}\right)^2\right]h_1 + \left(\pi\rho A_{12}\right)h_2 + \left(\pi\rho A_{13}\right)h_3$$
$$+\left(\pi\rho A_{14} + S_{\alpha_{11}}\right)\alpha_1 + \left(\pi\rho A_{15} + S_{\alpha_{12}}\right)\alpha_2 = 0$$

$$\left(\pi\rho A_{21}\right)h_1 + \left[\pi\rho A_{22} + M_2 - M_2\left(1 + ig_{h_2}\right)\left(\frac{\omega_{h_2}}{\omega}\right)^2\right]h_2 + \left(\pi\rho A_{23}\right)h_3$$
$$+\left(\pi\rho A_{24} + S_{\alpha_{21}}\right)\alpha_1 + \left(\pi\rho A_{25} + S_{\alpha_{22}}\right)\alpha_2 = 0$$

$$\left(\pi\rho A_{31}\right)h_1 + \left(\pi\rho A_{32}\right)h_2 + \left[\pi\rho A_{33} + M_3 - M_3\left(1 + ig_{h_3}\right)\left(\frac{\omega_{h_3}}{\omega}\right)^2\right]h_3$$
$$+\left(\pi\rho A_{34} + S_{\alpha_{31}}\right)\alpha_1 + \left(\pi\rho A_{35} + S_{\alpha_{32}}\right)\alpha_2 = 0$$

$$\left(\pi\rho A_{41} + S_{\alpha_{11}}\right)h_1 + \left(\pi\rho A_{42} + S_{\alpha_{21}}\right)h_2 + \left(\pi\rho A_{43} + S_{\alpha_{31}}\right)h_3$$
$$+\left[\pi\rho A_{44} + I_{\alpha_1} - I_{\alpha_1}\left(1 + ig_{\alpha_1}\right)\left(\frac{\omega_{\alpha_1}}{\omega}\right)^2\right]\alpha_1 + \pi\rho A_{45}\alpha_2 = 0$$

$$\left(\pi\rho A_{51} + S_{\alpha_{12}}\right)h_1 + \left(\pi\rho A_{52} + S_{\alpha_{22}}\right)h_2 + \left(\pi\rho A_{53} + S_{\alpha_{32}}\right)h_3$$
$$+\pi\rho A_{54}\alpha_1 + \left[\pi\rho A_{55} + I_{\alpha_2} - I_{\alpha_2}\left(1 + ig_{\alpha_2}\right)\left(\frac{\omega_{\alpha_2}}{\omega}\right)^2\right]\alpha_2 = 0$$

The five equations to the flutter problem can be written in matrix form as

(6)

$$\begin{bmatrix} \left[\pi\rho A_{11}+M_1-M_1\left(1+ig_{h_1}\right)\left(\frac{\omega_{h_1}}{\omega}\right)^2\right] & \pi\rho A_{12} & \pi\rho A_{13} & \pi\rho A_{14}+S_{\alpha_{11}} & \pi\rho A_{15}+S_{\alpha_{12}} \\ \pi\rho A_{21} & \left[\pi\rho A_{22}+M_2-M_2\left(1+ig_{h_2}\right)\left(\frac{\omega_{h_2}}{\omega}\right)^2\right] & \pi\rho A_{23} & \pi\rho A_{24}+S_{\alpha_{21}} & \pi\rho A_{25}+S_{\alpha_{22}} \\ \pi\rho A_{31} & \pi\rho A_{32} & \left[\pi\rho A_{33}+M_3-M_3\left(1+ig_{h_3}\right)\left(\frac{\omega_{h_3}}{\omega}\right)^2\right] & \pi\rho A_{34}+S_{\alpha_{31}} & \pi\rho A_{35}+S_{\alpha_{32}} \\ \pi\rho A_{41}+S_{\alpha_{11}} & \pi\rho A_{42}+S_{\alpha_{21}} & \pi\rho A_{43}+S_{\alpha_{31}} & \left[\pi\rho A_{44}+I_{\alpha_1}-I_{\alpha_1}\left(1+ig_{\alpha_1}\right)\left(\frac{\omega_{\alpha_1}}{\omega}\right)^2\right] & \pi\rho A_{45} \\ \pi\rho A_{51}+S_{\alpha_{12}} & \pi\rho A_{52}+S_{\alpha_{22}} & \pi\rho A_{53}+S_{\alpha_{32}} & \pi\rho A_{54} & \left[\pi\rho A_{55}+I_{\alpha_2}-I_{\alpha_2}\left(1+ig_{\alpha_2}\right)\left(\frac{\omega_{\alpha_2}}{\omega}\right)^2\right] \end{bmatrix} \begin{bmatrix} h_1 \\ h_2 \\ h_3 \\ \alpha_1 \\ \alpha_2 \end{bmatrix} = 0$$

4. Eigenvalues

Equation (6) is a complex eigenvalue problem. In order to solve the flutter problem, it is convenient to rewrite the problem in the form $\left(\bar{A}-IZ\right)X=0$ by arbitrarily letting

$$Z=\left(\frac{\omega_{\alpha_1}}{\omega}\right)^2\left(1+ig\right),$$

which results in

$$\begin{vmatrix} \bar{A}_{11}-Z & \bar{A}_{12} & \bar{A}_{13} & \bar{A}_{14} & \bar{A}_{15} \\ \bar{A}_{21} & \bar{A}_{22}-Z & \bar{A}_{23} & \bar{A}_{24} & \bar{A}_{25} \\ \bar{A}_{31} & \bar{A}_{32} & \bar{A}_{33}-Z & \bar{A}_{34} & \bar{A}_{35} \\ \bar{A}_{41} & \bar{A}_{42} & \bar{A}_{43} & \bar{A}_{44}-Z & \bar{A}_{45} \\ \bar{A}_{51} & \bar{A}_{52} & \bar{A}_{53} & \bar{A}_{54} & \bar{A}_{55}-Z \end{vmatrix} = 0$$

The determinant elements are defined as:

$$\bar{A}_{11} = \left(\frac{\pi\rho A_{11}}{M_1} + 1 \right) \left(\frac{\omega_{\alpha_1}}{\omega_{h_1}} \right)^2 \qquad \bar{A}_{12} = \left(\frac{\pi\rho A_{12}}{M_1} \right) \left(\frac{\omega_{\alpha_1}}{\omega_{h_1}} \right)^2 \tag{7}$$

$$\bar{A}_{13} = \left(\frac{\pi\rho A_{13}}{M_1} \right) \left(\frac{\omega_{\alpha_1}}{\omega_{h_1}} \right)^2 \qquad \bar{A}_{14} = \left(\frac{\pi\rho A_{14} + S_{\alpha_{11}}}{M_1} \right) \left(\frac{\omega_{\alpha_1}}{\omega_{h_1}} \right)^2$$

$$\bar{A}_{15} = \left(\frac{\pi\rho A_{15} + S_{\alpha_{12}}}{M_1} \right) \left(\frac{\omega_{\alpha_1}}{\omega_{h_1}} \right)^2$$

$$\bar{A}_{21} = \left(\frac{\pi\rho A_{21}}{M_2} \right) \left(\frac{\omega_{\alpha_1}}{\omega_{h_2}} \right)^2 \qquad \bar{A}_{22} = \left(\frac{\pi\rho A_{22}}{M_2} + 1 \right) \left(\frac{\omega_{\alpha_1}}{\omega_{h_2}} \right)^2$$

$$\bar{A}_{23} = \left(\frac{\pi\rho A_{23}}{M_2} \right) \left(\frac{\omega_{\alpha_1}}{\omega_{h_2}} \right)^2 \qquad \bar{A}_{24} = \left(\frac{\pi\rho A_{24} + S_{\alpha_{21}}}{M_2} \right) \left(\frac{\omega_{\alpha_1}}{\omega_{h_2}} \right)^2$$

$$\bar{A}_{25} = \left(\frac{\pi\rho A_{25} + S_{\alpha_{22}}}{M_2} \right) \left(\frac{\omega_{\alpha_1}}{\omega_{h_2}} \right)^2$$

$$\bar{A}_{31} = \left(\frac{\pi\rho A_{31}}{M_3} \right) \left(\frac{\omega_{\alpha_1}}{\omega_{h_3}} \right)^2 \qquad \bar{A}_{32} = \left(\frac{\pi\rho A_{32}}{M_3} \right) \left(\frac{\omega_{\alpha_1}}{\omega_{h_3}} \right)^2$$

$$\bar{A}_{33} = \left(\frac{\pi\rho A_{33}}{M_3} + 1 \right) \left(\frac{\omega_{\alpha_1}}{\omega_{h_3}} \right)^2 \qquad \bar{A}_{34} = \left(\frac{\pi\rho A_{34} + S_{\alpha_{31}}}{M_3} \right) \left(\frac{\omega_{\alpha_1}}{\omega_{h_3}} \right)^2$$

$$\bar{A}_{35} = \left(\frac{\pi\rho A_{35} + S_{\alpha_{32}}}{M_3} \right) \left(\frac{\omega_{\alpha_1}}{\omega_{h_3}} \right)^2$$

$$\bar{A}_{41} = \left(\frac{\pi\rho A_{41} + S_{\alpha_{11}}}{I_{\alpha_1}} \right) \qquad \bar{A}_{42} = \left(\frac{\pi\rho A_{42} + S_{\alpha_{21}}}{I_{\alpha_1}} \right)$$

$$\bar{A}_{43} = \left(\frac{\pi\rho A_{43} + S_{\alpha_{31}}}{I_{\alpha_1}} \right) \qquad \bar{A}_{44} = \left(\frac{\pi\rho A_{44}}{I_{\alpha_1}} + 1 \right)$$

$$\bar{A}_{45} = \left(\frac{\pi \rho A_{45}}{I_{\alpha_1}} \right)$$

$$\bar{A}_{51} = \left(\frac{\pi \rho A_{51} + S_{\alpha_{12}}}{I_{\alpha_2}} \right) \left(\frac{\omega_{\alpha_1}}{\omega_{\alpha_2}} \right)^2 \qquad \bar{A}_{52} = \left(\frac{\pi \rho A_{52} + S_{\alpha_{22}}}{I_{\alpha_2}} \right) \left(\frac{\omega_{\alpha_1}}{\omega_{\alpha_2}} \right)^2$$

$$\bar{A}_{53} = \left(\frac{\pi \rho A_{53} + S_{\alpha_{32}}}{I_{\alpha_2}} \right) \left(\frac{\omega_{\alpha_1}}{\omega_{\alpha_2}} \right)^2 \qquad \bar{A}_{54} = \left(\frac{\pi \rho A_{54}}{I_{\alpha_2}} \right) \left(\frac{\omega_{\alpha_1}}{\omega_{\alpha_2}} \right)^2$$

$$\bar{A}_{55} = \left(\frac{\pi \rho A_{55}}{I_{\alpha_2}} + 1 \right) \left(\frac{\omega_{\alpha_1}}{\omega_{\alpha_2}} \right)^2$$

It should be noted that the coefficients of the characteristic equation of the $\left(\bar{A} - IZ\right)$ matrix (a quintic in Z) are complex, due to Theodorsen's lift deficiency function, and thus the eigenvalues will be complex. The coupled frequency of oscillation (ω) for each eigenvalue can be found from the real part of Z, since the first torsional natural frequency is already known:

$$\omega_i = \frac{\omega_{\alpha_1}}{\sqrt{\mathrm{Re}(Z)}}$$

The damping coefficient required for flutter to exist (g) for each eigenvalue can be found from the imaginary part of Z:

$$g_i = \mathrm{Im}(Z) \left(\frac{\omega_i}{\omega_{\alpha_1}} \right)^2$$

If *g* is negative for the reduced frequency chosen, then damping must be decreased in order to obtain flutter. Negative values of *g* represent the stable, or non-flutter, condition. If *g* is positive, then damping must be increased to be at the flutter point. Positive values of g represent the unstable, or flutter condition. When a plot of g is made against 1/k (k being reduce frequency), there will be five curves corresponding to the variation of each eigenvalue as the reduced frequency varies. Some of these curves will have only values of g that are negative. These are the non-critical curves that

represent stable coupled modes and do not influence the flutter solution. However, at least one curve will start with a negative value of g and then at some point cross the abscissa (1/k) to a positive value of g. This curve is called the critical curve, and the value of 1/k where this curve crosses the abscissa represents the critical flutter speed, or flutter point. The critical flutter speed is found from the relationship:

$$U_{FL} = \frac{\omega b}{k_{crit}}$$

where ω is found from the real part of the eigenvalue relationship described above for the critical curve evaluated at the reduced frequency that corresponds to the crossover point (k_{crit}). Once the unstable mode is identified, results are commonly plotted as g vs. U_{FL}.

THIS PAGE INTENTIONALLY LEFT BLANK

III. RESULTS

A. UH-60 BLADE EXAMPLE

Using the data accumulated by NASA for Sikorsky's UH-60, a sample numerical problem will now be presented. The UH-60's blade is modeled as a uniform beam, incorporating the average geometric and inertial characteristics of the blade between 20% and 90% of its length. The flutter determinant for the blade is repeatedly solved for multiple elements along the blade model, as well as a range of forward velocities, in the conventional manner to obtain the blade flutter speed [Ref. 8]. UH-60 blade parameters will be used in the sample problem in deference to the extensive database now available for this blade. However, for the demonstration analysis the UH-60 blade will be modified to make it "flutter susceptible" by moving the chord-wise position of the blade CG aft while keeping its elastic axis at the quarter chord. This also introduces flap torsion coupling, a desirable feature for a sample problem of this type.

For the numerical example, the blade will be divided into radial segments in the usual manner with unsteady aerodynamics applied to the blade at each panel point. The number of elements chosen has some effect on the accuracy of the solution, since the variation of velocity along the span must be adequately incorporated. Through trial and error, it has been found that the change in flutter point as the number of elements exceeds 50 is insignificant (<1%), while using only 5 or 10 elements can give variations as great as 10%.

Physically, the method of solution in this thesis is equivalent to locking the blade at the 90-degree azimuth position and solving the flutter problem, similar to a fixed wing case with Theodorsen lift deficiency values, yet allowing radial velocity, and thus, reduced frequency, to vary with span as in the case of the tangential velocity of a rotor blade in forward flight, $\psi = 90^{\circ}$.

The average characteristics of the H-60 rotor blade are given in Table 1 [Ref. 15]. Scanlan and Rosenbaum [Ref. 8] state that any mode with a natural frequency greater than 1.2 times the frequency of the first torsion mode will not have a significant effect on the flutter point. The third bending mode (>7.5Ω) and the second torsion mode (>11Ω) are both significantly outside this range.

Table 1. UH-60 Blade Characteristics

PARAMETER	VALUE	UNITS
M	0.00164	lb-s^2/in^2
C	20.76	in
I_α	0.037	lb-s^2-in/in
R	322	in
E	15	in
EA	25% chord	
CG	Variable	
Ω	27.02	rad/s
ΩR	725	ft/s

Hence, only the first two flap-wise bending modes with natural frequencies of 2.8Ω and 4.7Ω are incorporated in the flutter analysis together with one torsion mode, occurring at 4.3Ω. The rotating natural frequencies of the uniform beam model are compared to that of the real blade in Table 2. Note that the frequencies in each case are within 10% of the real values, giving confidence that the uniform beam model is sufficient for a first order approximation.

Table 2. Comparison of Rotating Natural Frequencies

MODE	BLADE MODEL	UH-60 BLADE
1st Bending	72.75	75.93
2nd Bending	130.47	140.23
1st Torsion	128.84	116.1

With the mode shapes and natural frequencies calculated, the flutter analysis portion of the program yielded results for a range of velocities for each CG location specified, from the quarter chord aft to the ¾ chord. After this analysis was conducted, it was done again, this time holding the forward velocity at zero and using the same tip velocity range as the forward flight case. This effort simulates whirl-stand over-speed tests. Figures 8 and 9 show the results of ω vs. U_{FL} and g vs. U_{FL} for both the forward velocity and over-speed cases with zero CG offset.

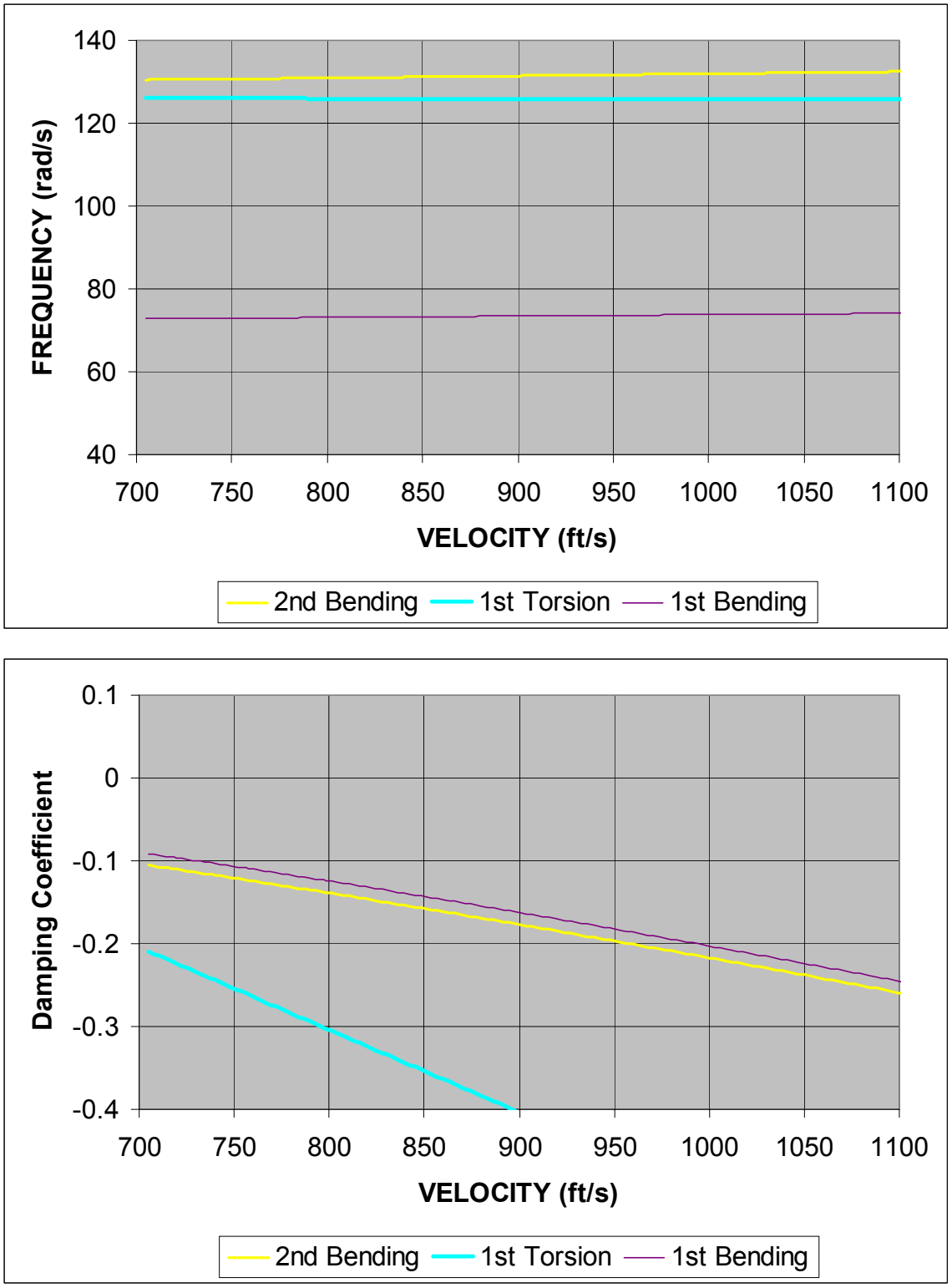

Figure 8. CG Offset Zero, Forward Flight

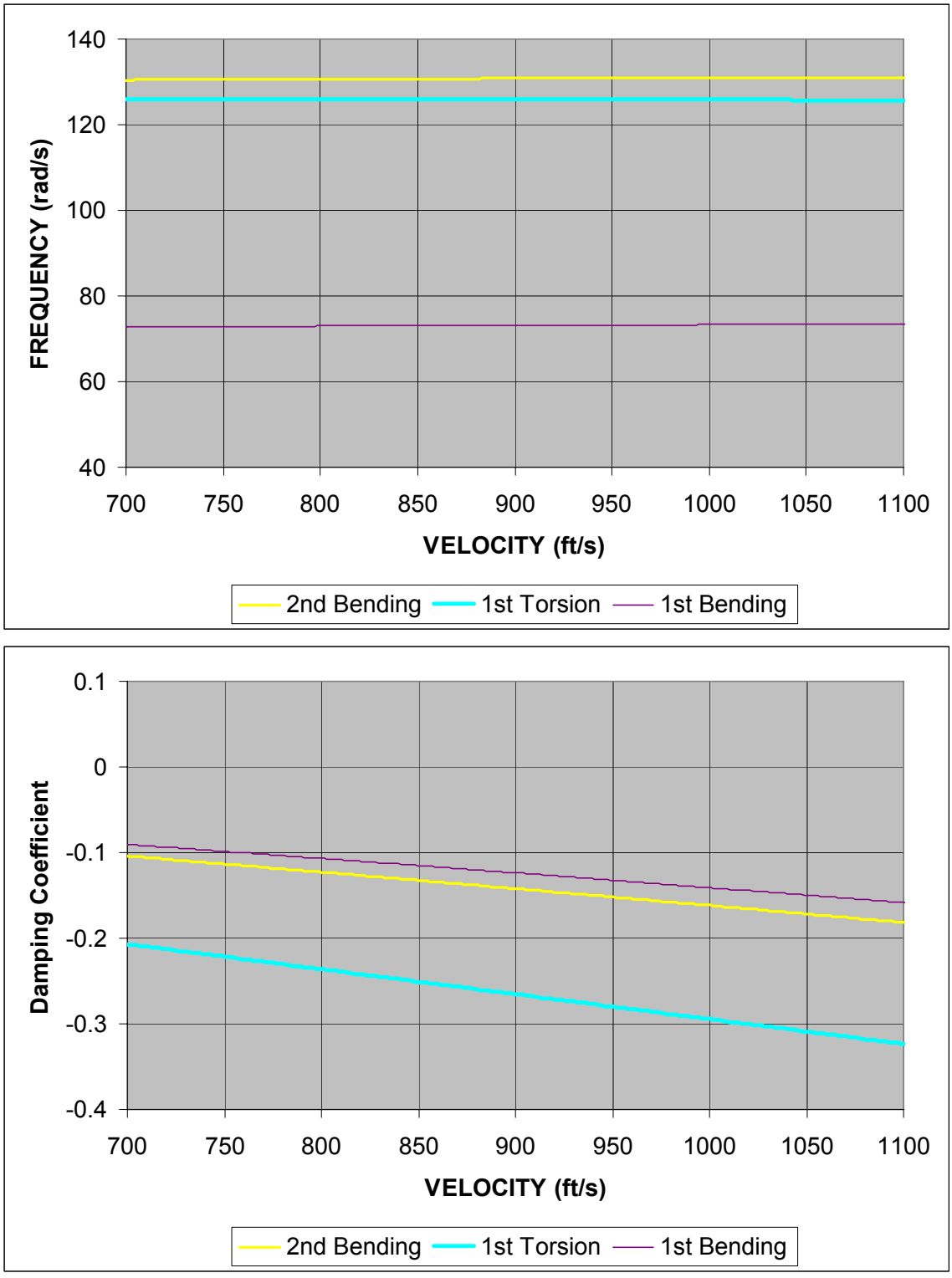

Figure 9. CG Offset Zero, Over-Speed

Note that the blade model is stable in both cases, with the natural frequencies remaining relatively constant, and the damping coefficients negative throughout the velocity range. Incidentally, the velocity range plotted is equivalent to the forward flight airspeeds of 0 – 220kts (approximately), which is the published flight envelope for the UH-60, plus 40kts.

Figures 10 through 21 show the progression of results, in the same format, as the CG is moved to the mid-chord position and subsequently aft to the ¾ chord position.

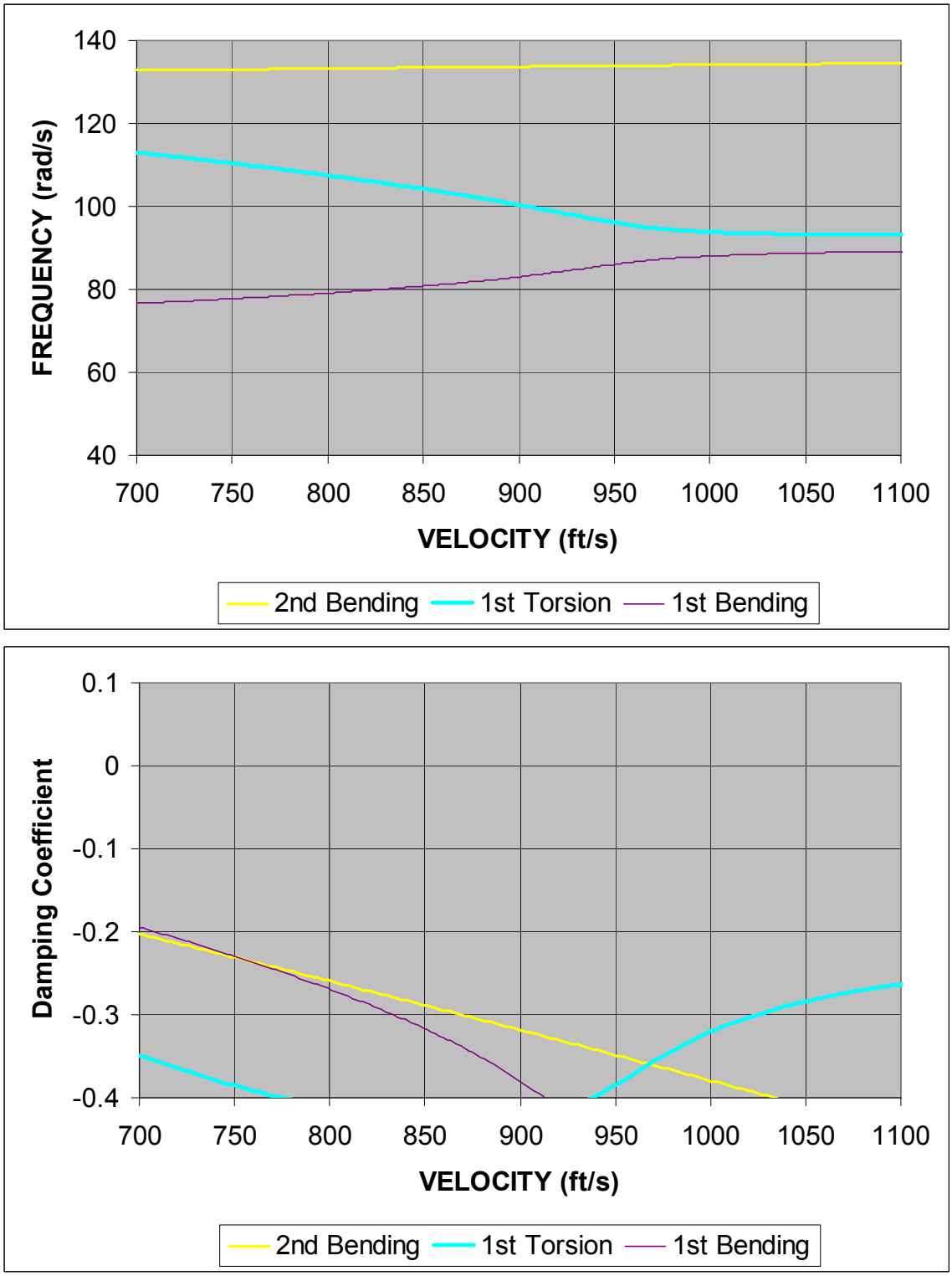

Figure 10. CG Offset 0.5b, Forward Flight

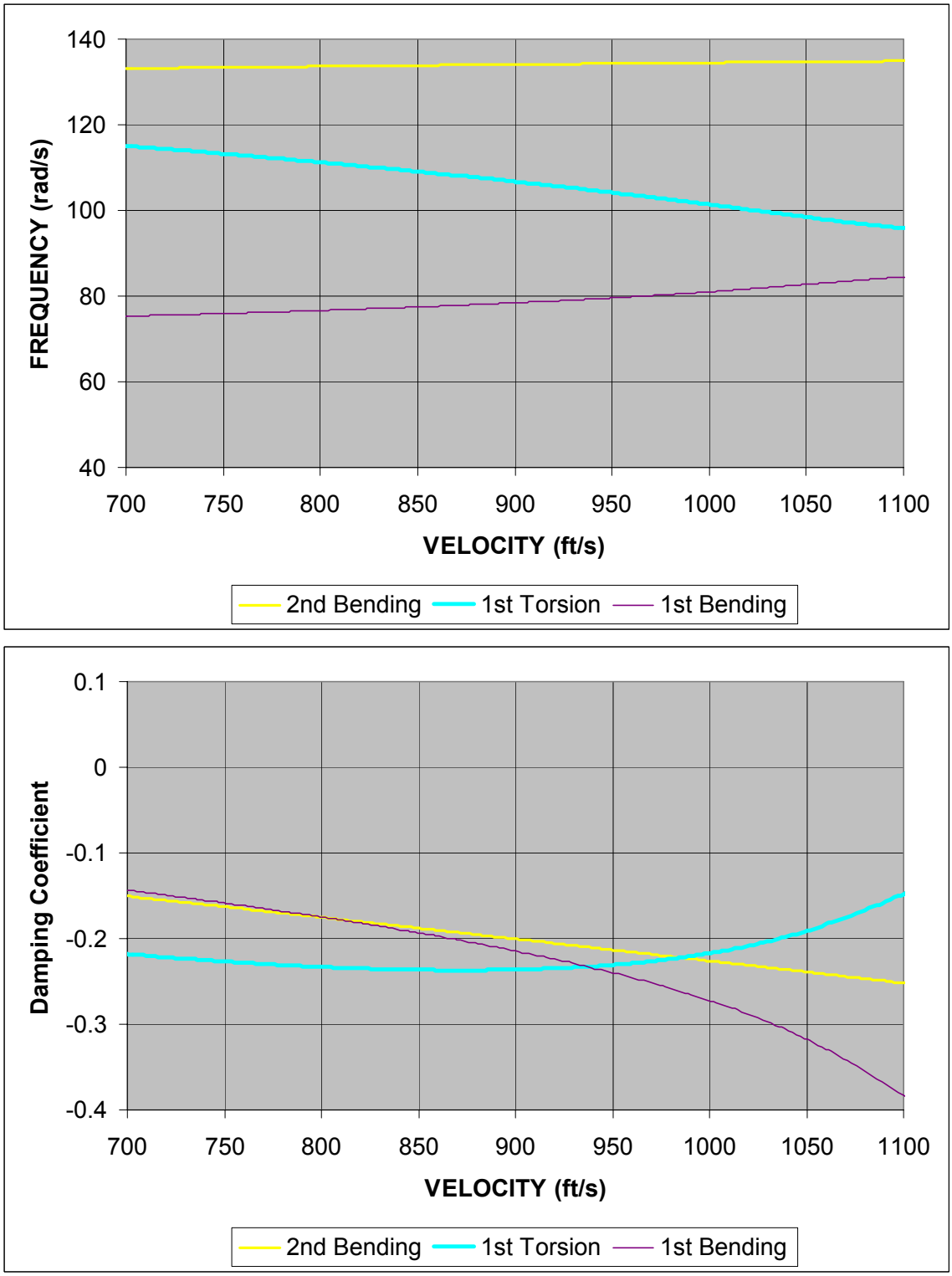

Figure 11. CG Offset 0.5b, Over-Speed

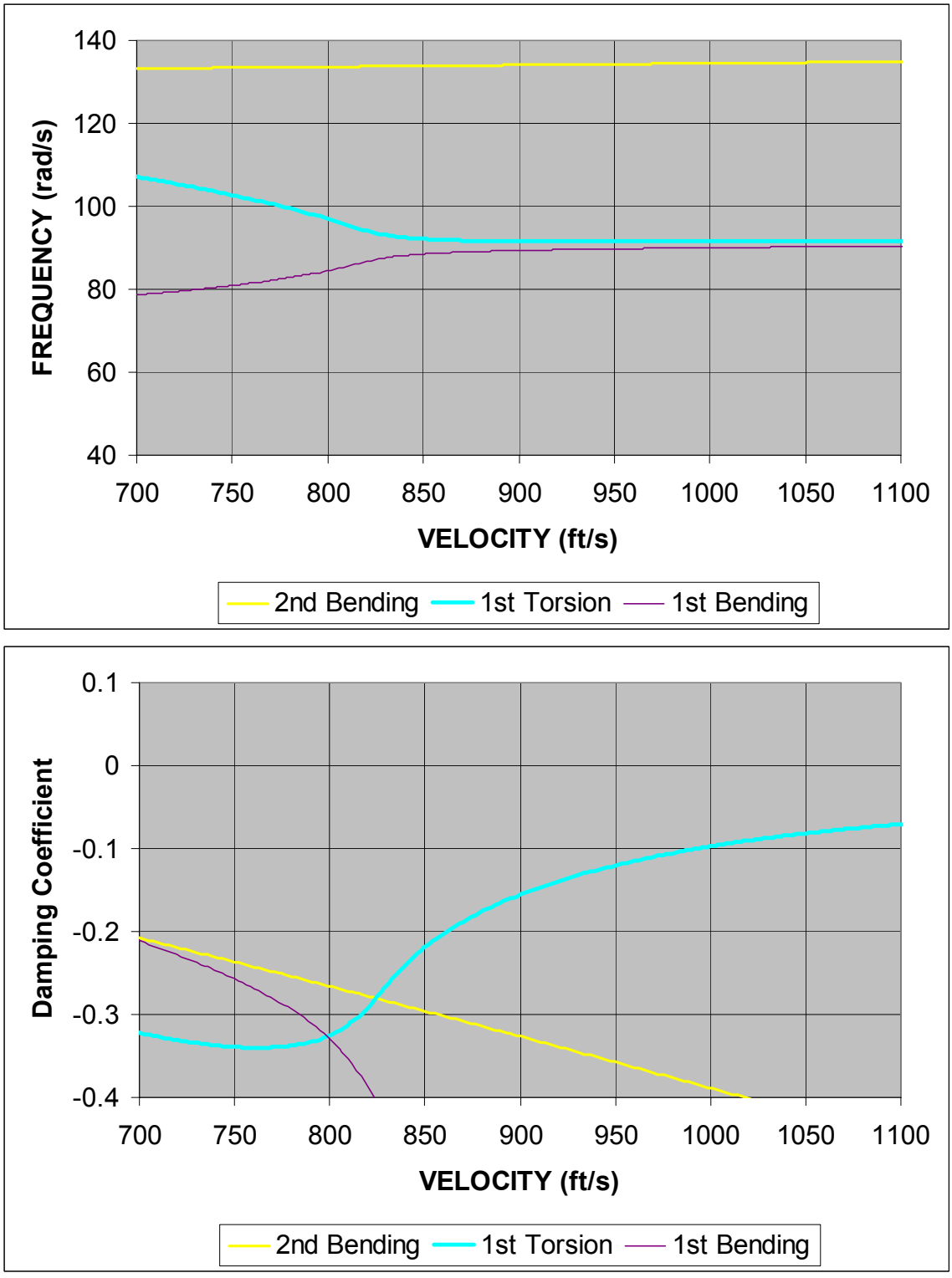

Figure 12. CG Offset 0.75b, Forward Flight

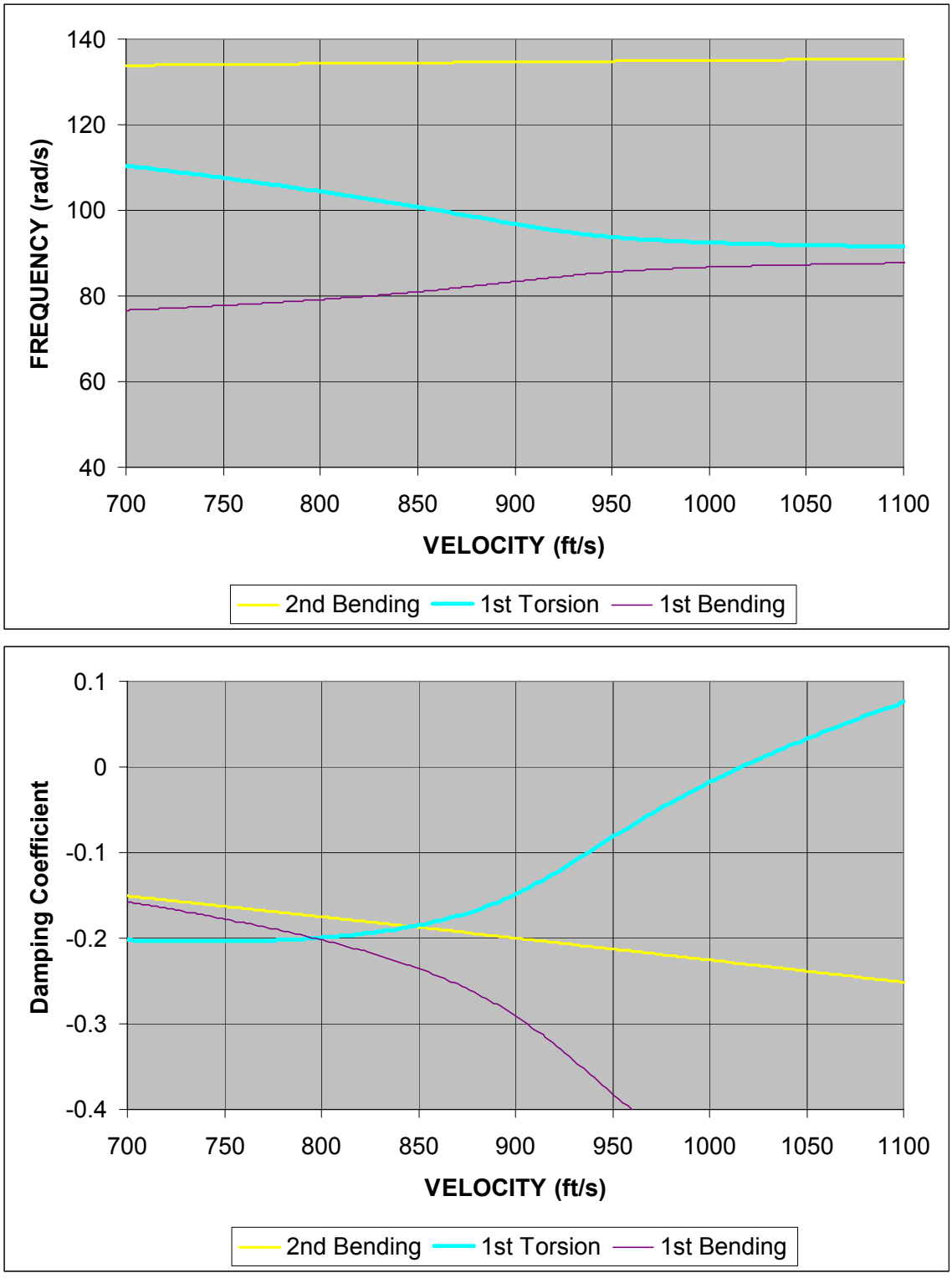

Figure 13. CG Offset 0.75b, Over-Speed

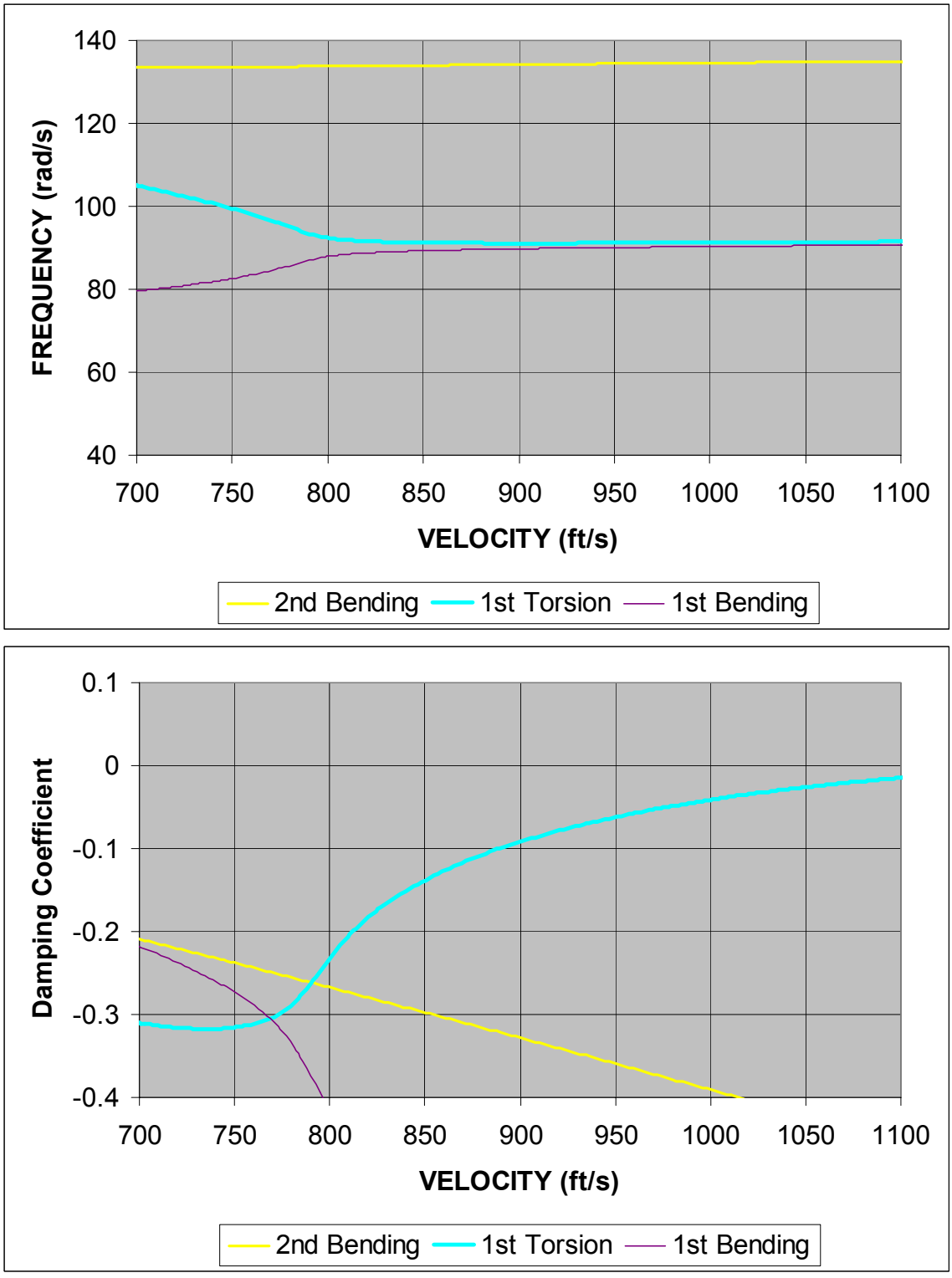

Figure 14. CG Offset 0.85b, Forward Flight

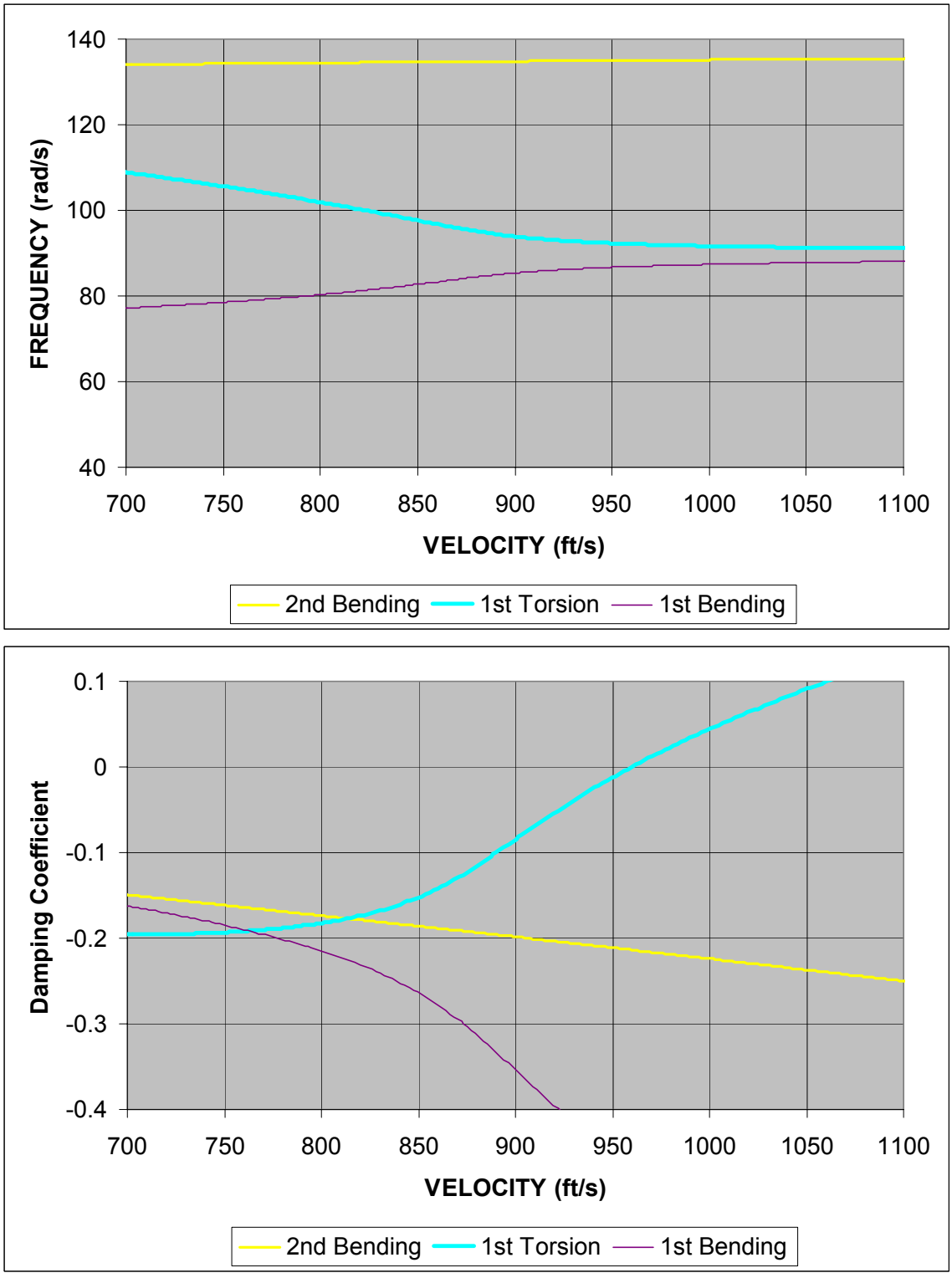

Figure 15. CG Offset O.85b, Over-Speed

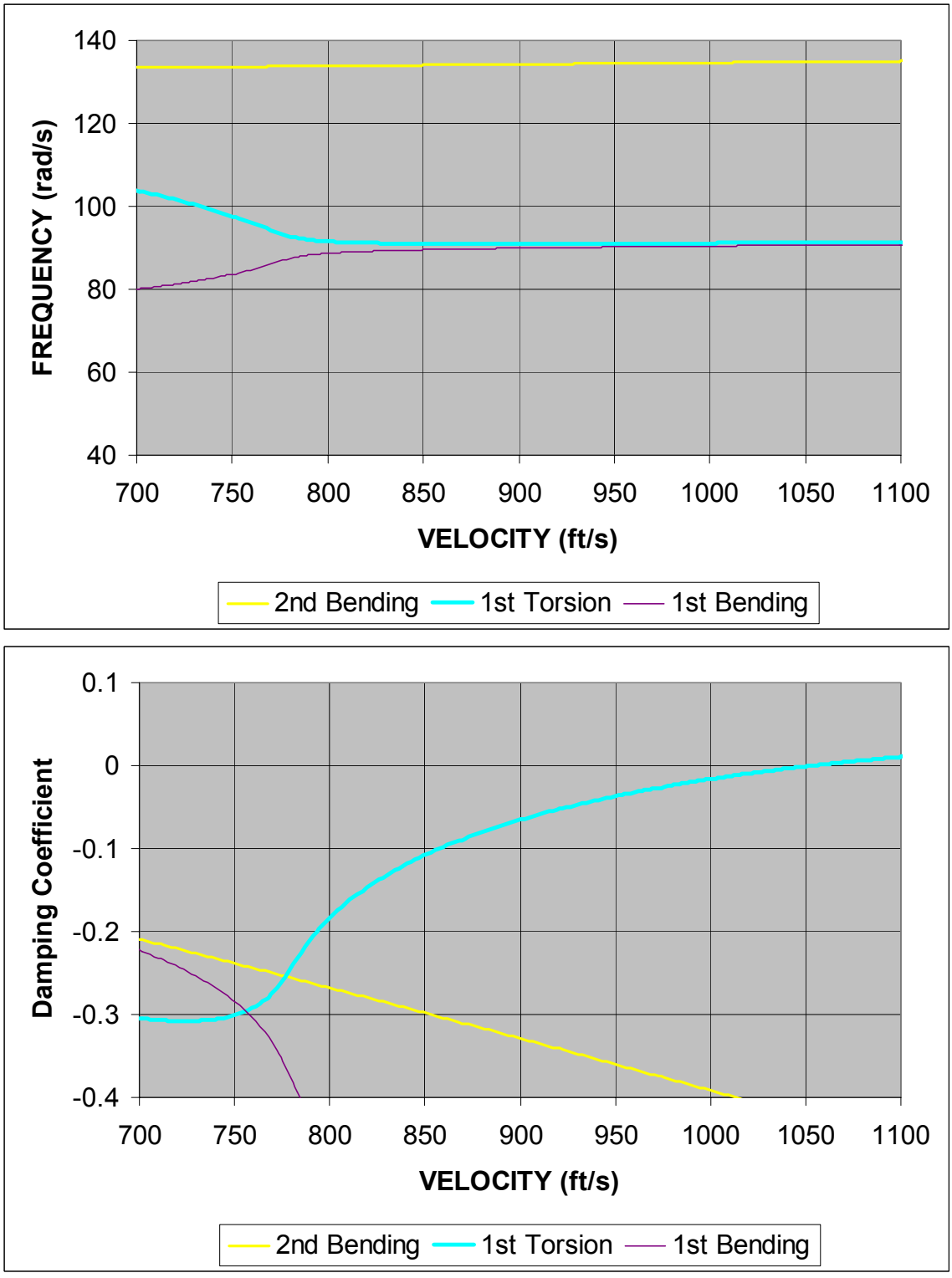

Figure 16. CG Offset 0.9b, Forward Flight

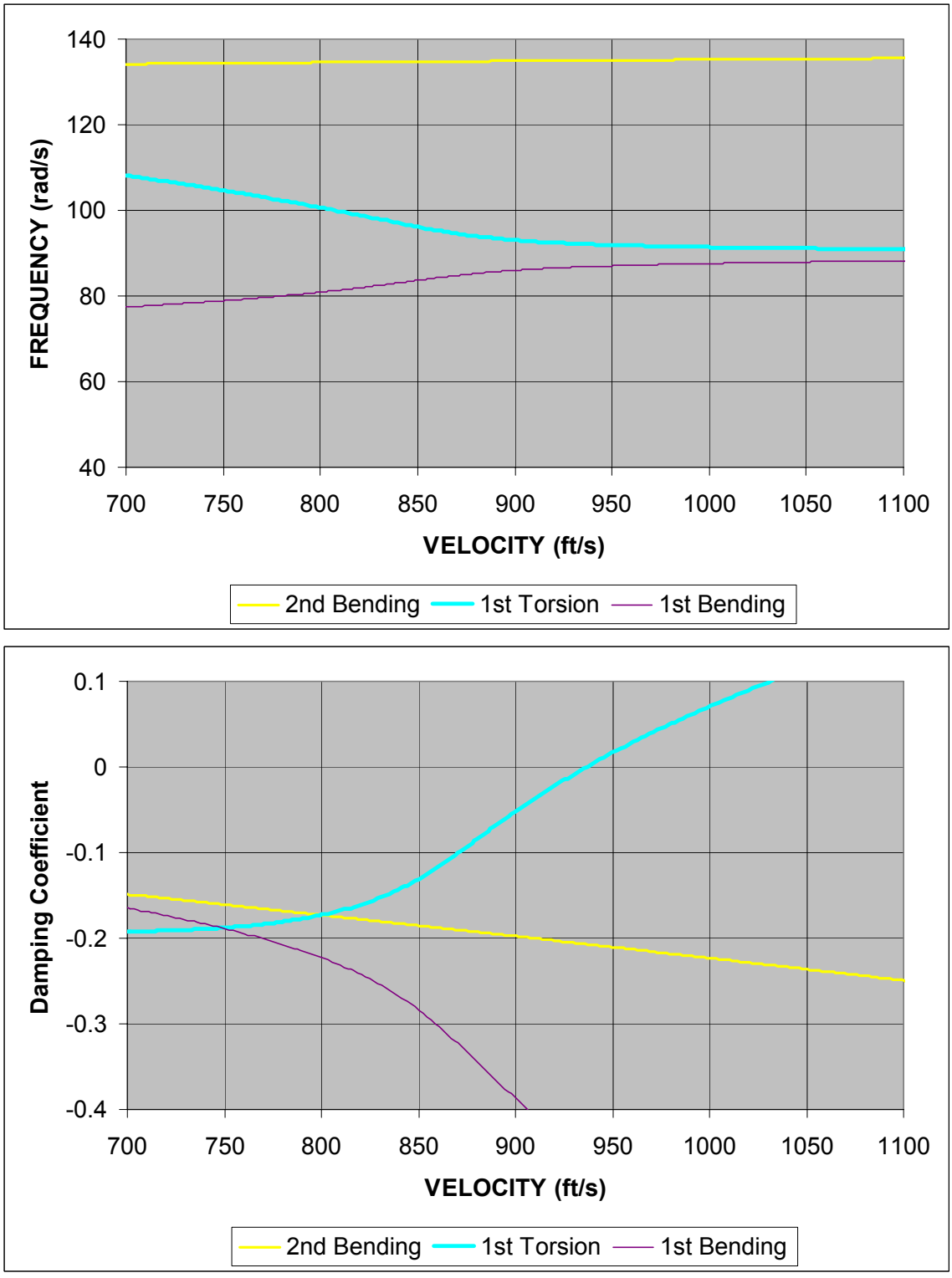

Figure 17. CG Offset O.9b, Over-Speed

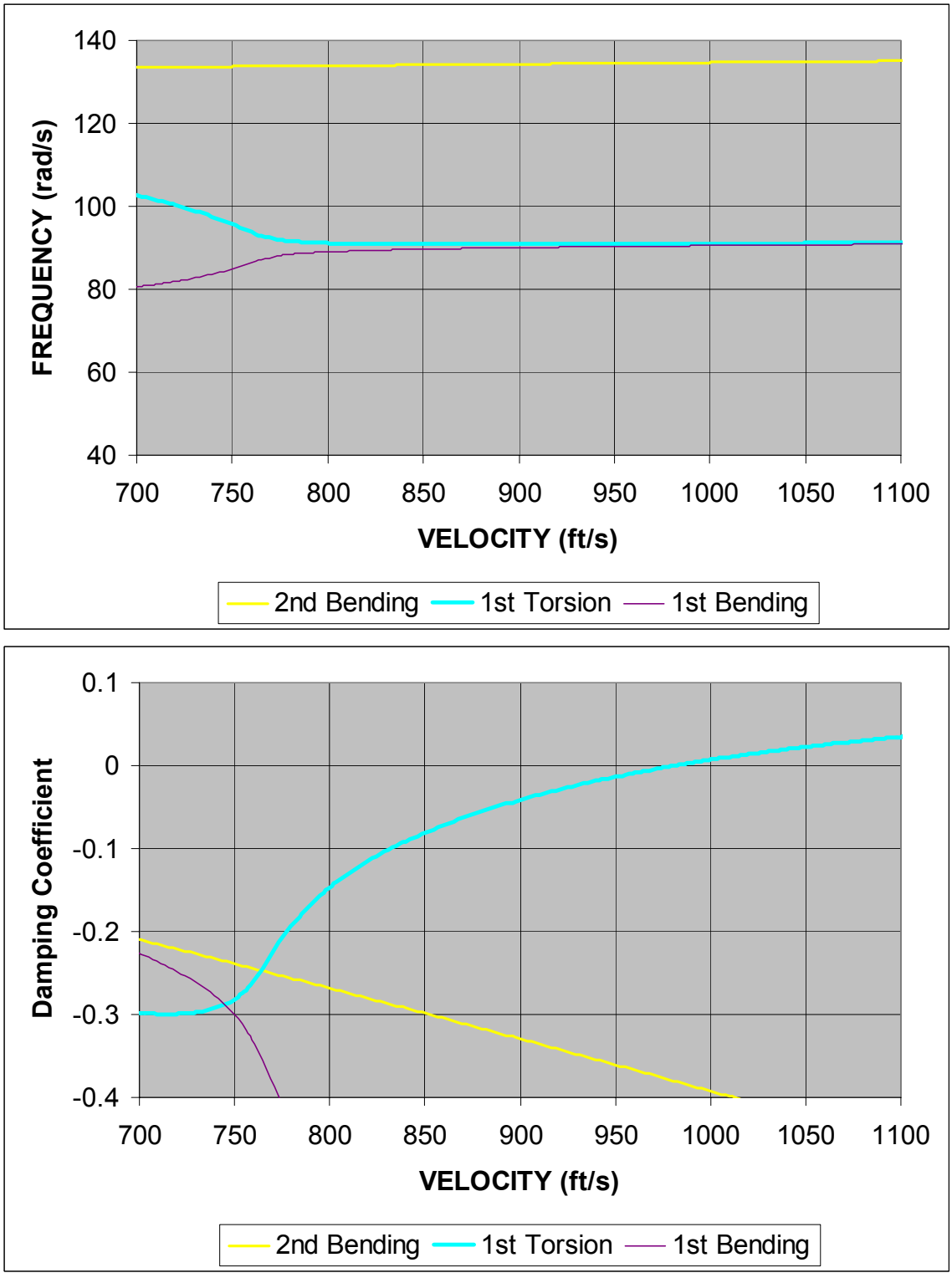

Figure 18. CG Offset 0.95b, Forward Flight

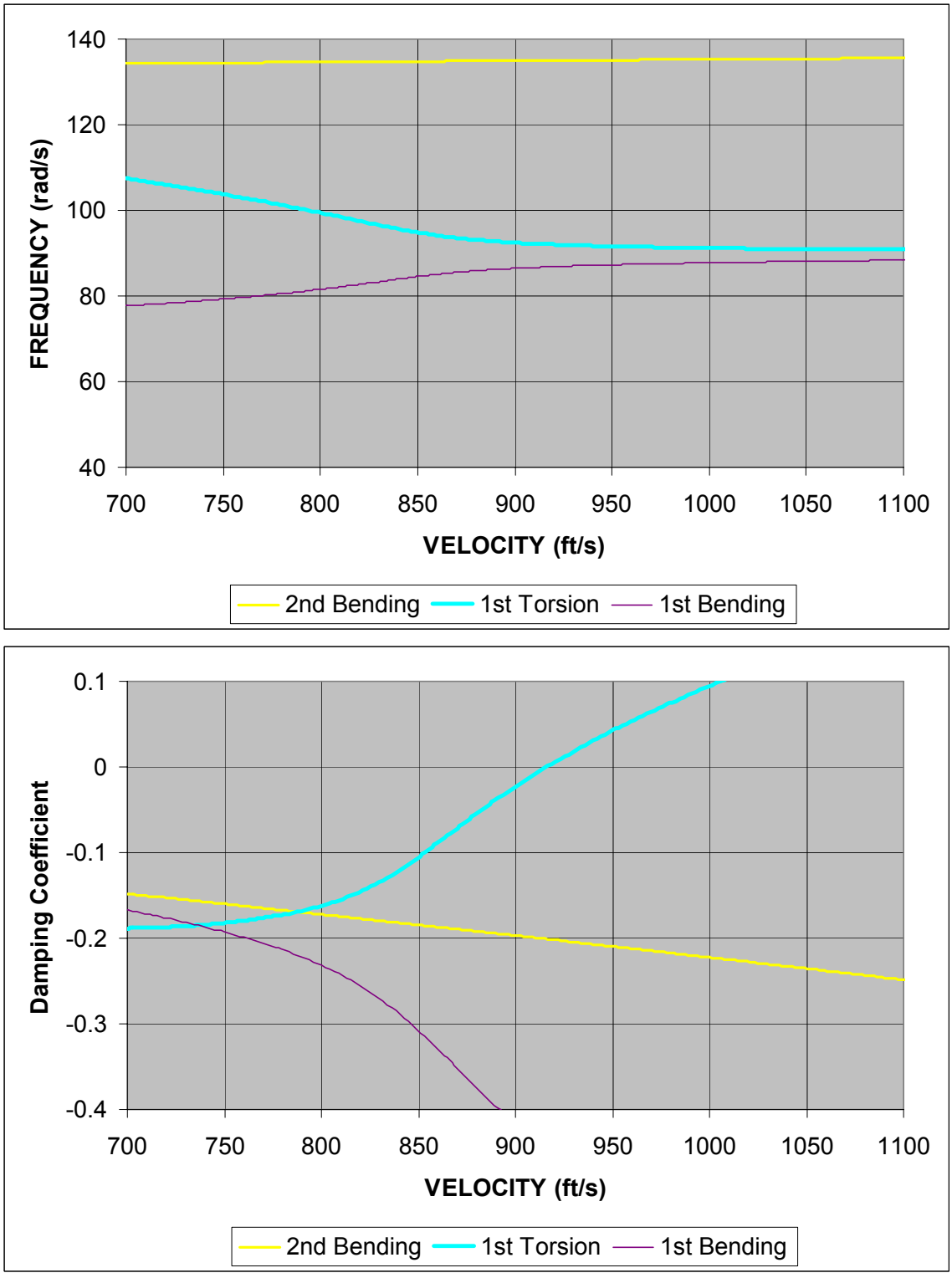

Figure 19. CG Offset O.95b, Over-Speed

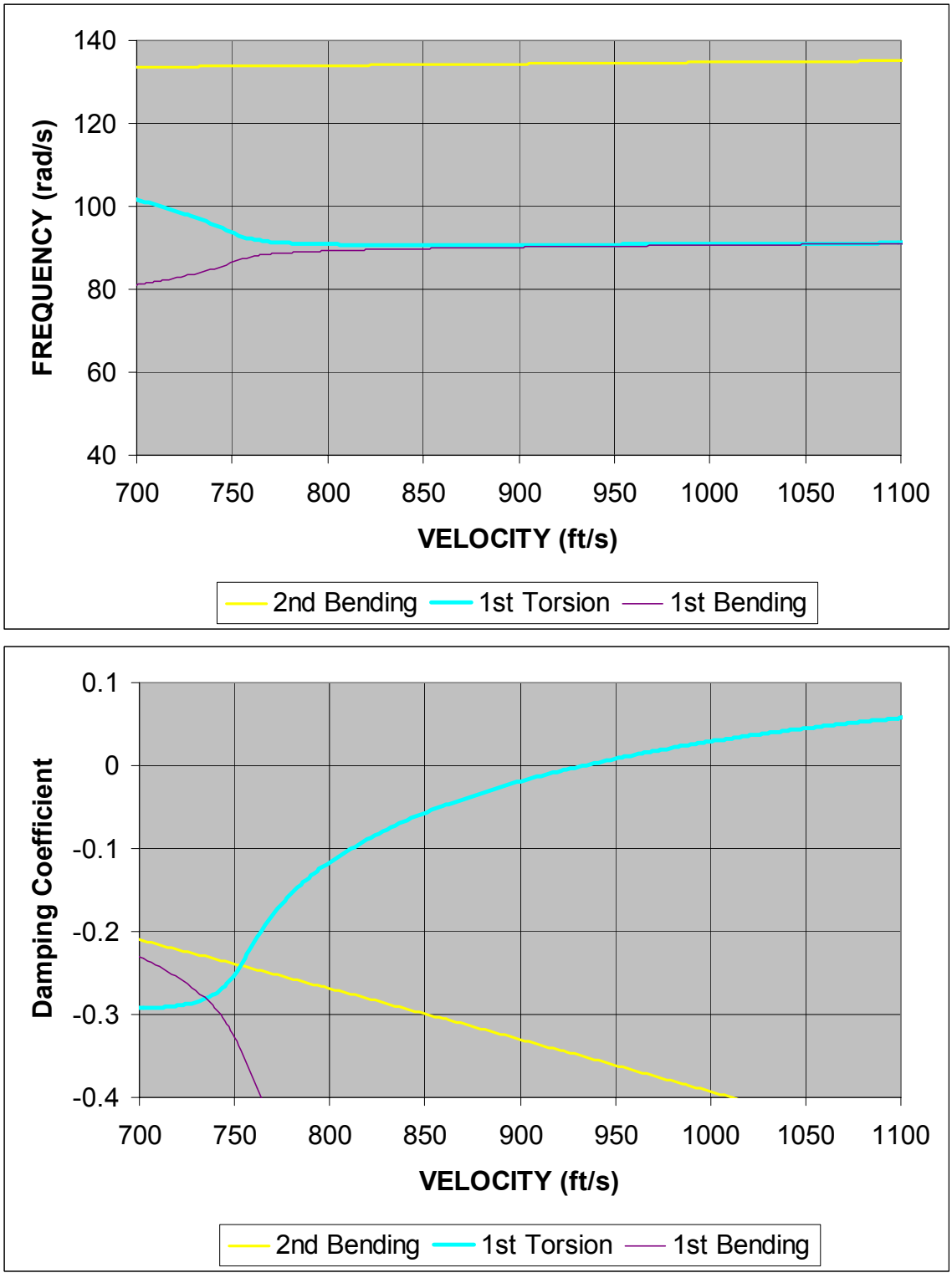

Figure 20. CG Offset 1.0b, Forward Flight

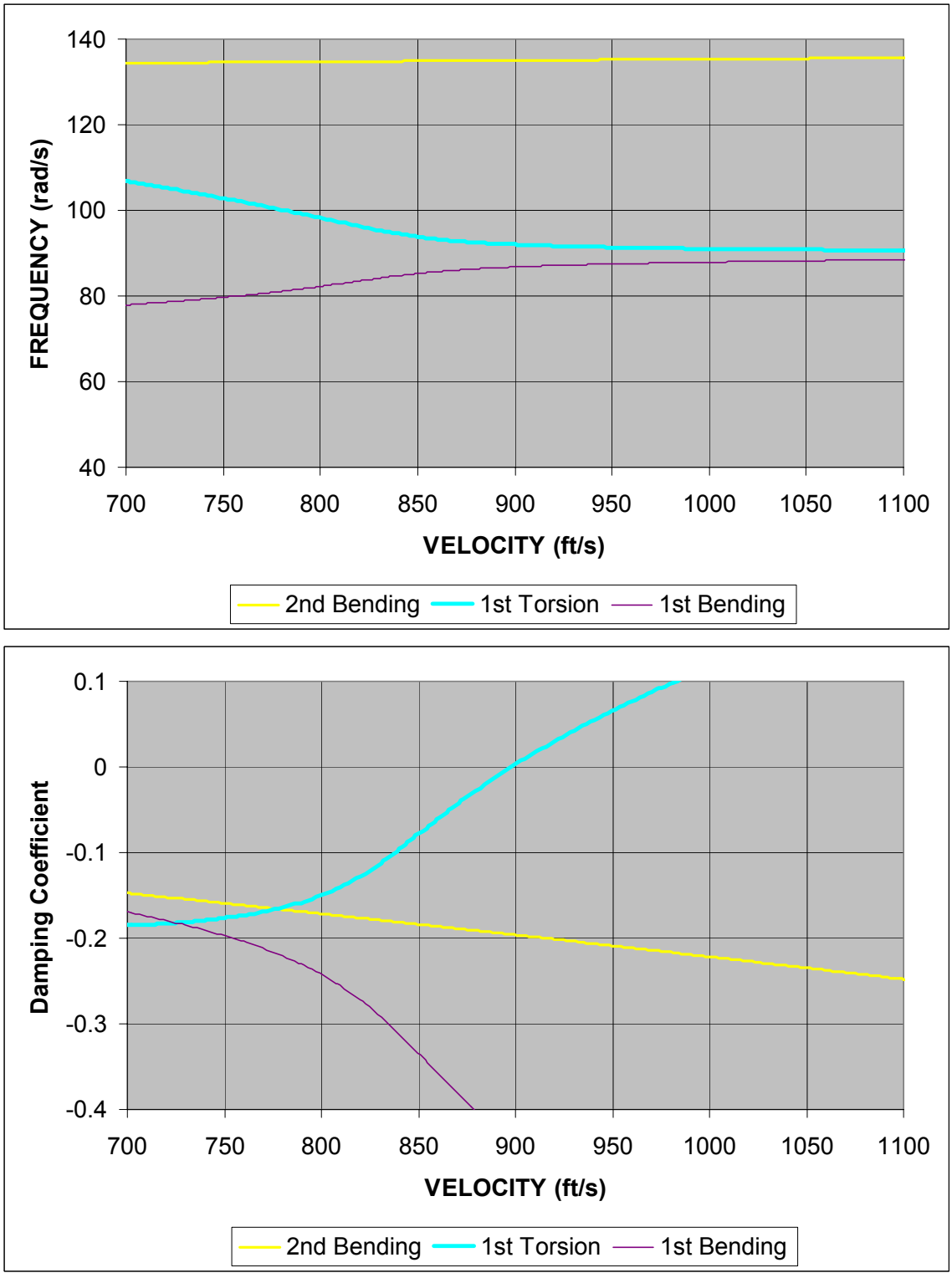

Figure 21. CG Offset 1.0b, Over-Speed

B. DISCUSSION OF RESULTS FOR UH-60 BLADE EXAMPLE

From Figures 10 and 11, it can be seen that the first two coupled modes, corresponding to the first bending and torsion modes, begin to converge in frequency, causing one of the modes to become more stable while the other becomes less stable. The movement of the damping coefficient curves, show this stability, or instability: larger negative values equals increased stability, and vice-versa. The first flutter point appears for the over-speed test at 1017ft/s tip speed, with the CG at 0.75b, or 62.5% chord. The forward flight curve is stable at this point. The forward flight condition remains stable until the CG is moved to the 0.9b position, or 70% chord. The tip speed for this case is 1054ft/s, corresponding to a forward flight velocity of 194kts. Note that the flutter point for each test occurs at a lower tip speed, as the CG is moved further aft. Table 3 provides a summary of the flutter points, for both the maximum forward flight velocity and maximum over-speed. The forward flight column lists the tip speed and forward velocity of the flutter point, and the over-speed column lists the flutter point tip speed.

Table 3. Flutter Points

CG Offset	CG (% chord)	Forward Flight	Over-speed
0.75b	62.5%	-	1017fps
0.85b	67.5%	-	960fps
0.90b	70.0%	1054fps / 194kts	937fps
0.95b	72.5%	981fps / 151kts	917fps
1.00b	75.0%	933fps / 123kts	893fps

IV. SUMMARY

A. CONCLUSIONS

This thesis has presented a fully coupled, quasi-3D analysis of rotor blade flutter that can accommodate forward flight conditions. The rotor blade is modeled as a uniform beam, taking the average characteristics of a real blade between 20% and 90% of its length. Applying Rayleigh's method, the first few bending and torsion normal mode shapes and natural frequencies are determined, and then adjusted for the rotating case. With this data, force and moment equations of motion are developed using LaGrange's equation along with a normal mode analysis. Theodorsen's lift deficiency function is calculated over a range of forward velocities, or reduced frequencies, for a specified number of elements along the blade model. Incorporating these coefficients into the equations of motion, a square matrix is generated from which complex eigenvalues can be derived. These eigenvalues provide the aeroelastic natural frequencies and damping coefficients for each coupled mode. The forward velocity at which one of the modes produces a damping coefficient of zero gives the value of reduced frequency for the flutter point. The resulting forward speed and blade tip speed can then be determined.

The results of this analysis appear to validate the methods used. The UH-60 model blade remains stable within a feasible forward velocity range (0 to 180kts) until the CG is moved aft of 70% chord. As the CG is moved aft, two of the coupled modes, corresponding to the first torsion and first bending modes, converge on a single frequency, approximately 91.8rad/s. As this convergence approaches, the mode corresponding to the first torsion mode becomes decreasingly stable, while the other becomes increasingly stable. Once the modes converge sufficiently, due to CG location, the coupled first torsion mode rapidly becomes unstable in the characteristic 'S-curve' manner. As a final indication of the validity of this analysis, the flutter point occurs at decreasing forward speeds as the CG is moved even further aft than the 70% chord point. The over-speed method of approximating forward flight flutter conditions, in contrast to the forward flight analysis presented above, seems to provide more conservative results.

The method presented in this thesis appears to be a valid and useful cost- and weight-saving tool for the rotor blade designer. This relatively simple approach can provide vital information for designing whirl-stand as well as flight tests of newly developed rotor blades, without being excessively conservative. The weight savings provided by allowing CG repositioning can be used to optimally weight the blade for better autorotative performance, or decreased design/weight/cost expenditures on blade damping. Altogether, further development of pre-existing flutter theory and unification with the power of modern computers allows advanced prediction without extensive cost.

B. RECOMMENDATIONS

Some of the simplifications made are not necessary, given the power and speed of modern computers. It should be noted that the simplifications of uniform blade and Yntema's method were used here to make possible rapid parametric studies. For detailed analysis of an actual rotor blade, the blade frequencies and mode shapes can be more accurately determined by a transfer matrix approach, such as the Mykelstad and/or Holtzer methods. In addition, the incorporation of more advanced lift deficiency functions, such as those developed by Loewy, and Shipman and Wood, which take into account the contributions of an unsteady wake, could further increase the accuracy of flutter prediction.

Another area to consider is that compressibility effects are not taken into account in spite of the fact that, even in a hover, the tip speed of most rotor blades is well into the compressible region. At high forward velocities, the tip speed often approaches Mach 1, and is likely to encounter transonic effects as well. The incorporation of compressibility effects promises to be challenging, but is likely to increase the accuracy of prediction.

APPENDIX A. 3D BLADE FLUTTER PROGRAM

A. PROGRAM WALK-THROUGH

A MATLAB™ program was written to conduct the flutter analysis using a uniform beam model of a real blade. MATLAB™ provides the user with the ability to make calculations simultaneously for large multi-dimensional matrices, making it appropriate for this subject matter. The steps of the program, along with an explanation of the methodology, follows:

1. Step 1 – User Input

The program begins by clearing the workspace variables. Then the user must choose the number of modes (3 or 5), the number of blade elements and the altitude (for air density variation). The separation between the CG and EA (positive for CG aft of EA) and the estimated forward velocity range must also be chosen. For the sample problem, a three-mode analysis was conducted over 100 blade elements at sea level.

2. Step 2 – Establish Blade Model Properties

The UH-60 blade was modeled as a uniform beam. The values chosen to represent the blade are the average values between 20% and 90% of the blade's length. Properties needed for this analysis include the mass per unit length (μ), Young's Modulus (E), the flap-wise (EI_{xx}) and polar (I_{α}) mass moments of inertia, and torsional stiffness (GJ). Throughout the program, the units of important quantities are denoted for clarification. In addition, this step establishes important aspects of the UH-60 such as rotor speed and blade offset, as well as the location of the elastic axis (in percent semi-chord from the mid-chord).

3. Step 3 – Calculate Mode Shapes and Natural Frequencies

This step establishes the elastic and inertial properties of the uniform beam and displays them, for comparison to real blade properties. First, the constants for the analysis are set. The references for these constants are noted in the program itself, and explained in the section on theoretical development. The beam is then divided into the user-specified number of elements, and the radii to the midpoints of the elements are calculated. The midpoints are the locations where the 2-D calculations will be made.

The mode shapes for bending and torsion are then calculated and normalized to a maximum deflection of one and a positive initial slope. These mode shapes are shown in Fig. 22. A small 'f' denotes a bending mode and a capital 'F' denotes a torsion mode.

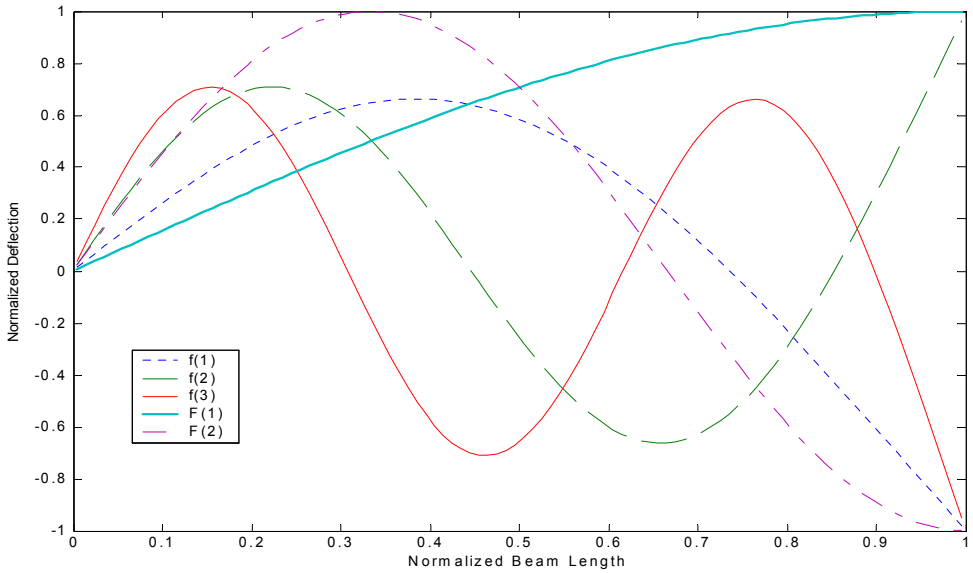

Figure 22. Normal Bending and Torsion Mode Shapes

The generalized mass for each mode is now calculated, using the mode shapes just obtained. The integral for the generalized masses is approximated by a summation as in the following example:

$$M_2 = \int_0^1 m(x)\left[f_2(x)\right]^2 dx = \sum_{n=1}^{p} \mu d f_2(n)$$

where p is the number of elements and d is the length of each element. Finally, the non-rotating and rotating natural frequencies are calculated with the equations above and displayed for comparison with values from the real blade.

4. Step 4 – Construct Matrices for Velocity Range

The fourth step is the heart of the program. This section begins the loop that calculates the matrix and its eigenvalues for each forward velocity. The range of velocities is set by the user's estimate and divided into 300 equally spaced velocities. This number seems to provide good resolution throughout the range of calculations. Next, a set of reduced frequencies is calculated using the semi-chord and the first torsion mode rotating natural frequency:

$$k_{tip} = \frac{b\omega_{\alpha_1}}{V_{fwd} + \Omega R}$$

This frequency is used as an approximation to the actual coupled frequency that is expected to become unstable and is only used as a means to obtain a reasonable range of reduced frequencies.

Following this, the static moment coupling terms must be calculated. Again, the integral is approximated with a summation as follows:

$$S_{\alpha_{12}} = \int_0^1 S_\alpha(x) f_1(x) F_2(x) dx = \sum_{n=1}^{p} S_\alpha(n) f_1(n) F_2(n) d$$

where p is the user-specified number of elements, and d is the length of each element.

Now the program is set to begin iterative calculations. For each step of forward velocity, Theodorsen coefficients are calculated for every element along the blade, according to the differing local velocities, and thus, reduced frequencies. Arrays are created of reduced frequencies, lift deficiency functions, and coefficients, corresponding to the array of element midpoints. Then, the matrix of integrals in equation set (5) is constructed as a set of summations in the same manner as previously noted. The program variable for this matrix is 'A'. The 'A' matrix is then modified to incorporate the dimensional quantities of air density, generalized mass, and coupled static moment, as well as the factor π. This matrix, denoted 'Adim,' is analogous to the matrix given in equation (6). Finally, the 'Adim' matrix is 're-dimensionalized' with the generalized masses and squared natural frequency ratios in order to generate eigenvalues of the

desired form. The resulting matrix, 'Abar' in the program, is the final five by five, generalized forces and moments given in equation set (7).

5. Step 5 – Calculate Eigenvalues

The user-specified number of modes must be accounted for before the eigenvalues can be calculated. If the user picks five modes, the full matrix will be used, but this currently yields a result that has one eigenvalues with a negative real part, which corresponds to an imaginary frequency that is not physically permissible. Therefore, the three-mode matrix must be used. Luckily, no further calculations need be made to enact this solution. A new matrix is formed from the 5 by 5 matrix by simply eliminating all terms with the subscripts 3 and 5, which correspond to the third bending mode and the second torsion mode, creating the appropriate 3 by 3 coupled matrix. Conveniently enough, it is noted in Scanlan and Rosenbaum [Ref. 7] that any mode with a natural frequency greater than 1.2 times the frequency of the first torsion mode will not have a significant effect on the flutter point. Both of the eliminated modes fall into this category.

Finally, the eigenvalues are calculated using MATLAB^{TM}'s 'eig' command. This command is executed without balancing in order to eliminate the possibility that a small value off the diagonal will be inordinately skewed in the balancing process. The eigenvalues are then sorted according to their real part and broken down into coupled frequencies and damping coefficients as discussed above.

6. Step 6 – Display Results and Save Data

The last step is to save and display the data in a useful manner. Recall that the values of reduced frequency were obtained using the natural frequency of the first torsion mode. However, the coupled frequency corresponding to the first torsion mode varies with velocity in a non-linear fashion. To obtain the actual velocity for each point calculated, the range of reduced frequencies must be divided into the semi-chord and the range of coupled (1st torsion mode) frequencies.

$$\left[V_{tip}\right] = \frac{b\left[\omega_2\right]}{\left[k_{tip}\right]}$$

Note that the division is conducted term by term, as an array.

The frequencies and damping ratios are then plotted versus this velocity such that the user can view the flutter point (damping coefficient 'g' = 0), if any. The data is also saved to a file for incorporation into a spreadsheet for further data analysis, as desired.

B. PROGRAM LISTING

```
%  Program to find natural static & rotating
%   mode shapes & frequencies of a uniform beam
%  Used to model the UH-60 rotor blade
%   (no aerodynamic effects taken into account)
%  Following frequency determination, all effects
%   are taken into account to determine
%   the flutter point (g=0 for one mode)
clear
mode=3;                              % input('5x5 (5) or 3x3 (3)?  ');
p=100;                               % input('How many elements?  ');
alt=0;                               % input('What altitude? (0, 5k, 10k) ');
cgea=input('CG - EA separation?  ');
mn=1;                                % input('Vfwd minimum? ');
mx=901;                               % input('Vfwd maximum? ');

R=322; offset=15; chord=20.76;       % inches
L=R-offset; e=offset/L;              % inches
O=27.02;                             % Rotor Speed rad/s
mu=0.00164167;                       % lbs^2/in^2
E=10000000;                          % lb/in^2
EIxx=2.27859e7; EIyy=7.71261e8;      % lbin^2
I=(EIxx+EIyy)/E;                     % in^4
Ia=0.037006386;                      % lbins^2/in  polar mass MOI about e.a.
GJ=2.467909e7;                       % lbin^2

a=-0.5;                      % non-dim elastic axis location measured from midchord
b=chord/2;                   % Half chord length in inches
if alt==10
   rho=0.0017556/(12^4);     % 10000 ft % lbs^2/in^4 density of air
elseif alt==5
   rho=0.0020482/(12^4);     % 5000 ft
else
   rho=0.0023769/(12^4);     % Sea Level
end
            % for rho = 0  AND  cg - ea = 0 : the natural frequencies are returned
```

```
asubn=[15.41820562 49.96486209 104.2476966];          % Hartog
K0=[6.38 17.63 35.05]; K1=[9.18 26.02 52.2];          % Yntema
BnR=[3.926602 7.068583 10.21018];        % Young/Felgar Free-Supported
An=[1.000777 1.000001 1];                % Young/Felgar Free-Supported

d=R/p;                          % length in inches of one element
Salf=mu*d*cgea*b;               % Calculate the static moment of each element

r(1)=0;                         % r is the vector of element edges in percent R
for q=1:p
   r(q+1)=q/p;
end
for n=1:p
   mid(n)=(r(n+1)+r(n))/2;      % midpoints of elements
end

u=mid'*BnR;                     % This section calculates the bending mode shapes
for n=1:3                       % According to Young and Felgar Supported-Free
   for m=1:p
      h=u(m,n);
      f(p+1-m,n)=(cosh(h)+cos(h)-An(n)*(sinh(h)+sin(h)))/2;
      % divide by two to normalize max deflection to one
   end
end

for n=1:3                       % This section normalizes mode shape
   if f(1,n)<0                  % to all begin with a positive slope
      h=-1*f(:,n);              % for display purposes
      f(:,n)=h;                 % (does not affect calculations)
   end
end

for n=1:3               % This section calculates the torsional mode shapes
   for m=1:p            % According to Hartog (already normalized to 1)
      F(m,n)=sin((n-.5)*pi*mid(m));
   end
end

figure(1)       % Plot of mode shapes
plot(mid,f(:,1),mid,f(:,2),mid,f(:,3),mid,F(:,1),mid,F(:,2))
legend('f(1)','f(2)','f(3)','F(1)','F(2)')

fSqr=f.*f;      % Calculate Generalized Mass for bending and torsion modes
FSqr=F.*F;
fMsqr=mu*d*fSqr;
FMsqr=d*Ia*FSqr;
```

```
Gmass=sum(fMsqr);
GTmass=sum(FMsqr);

oN=asubn*sqrt(EIxx/(mu*R^4));              % Calculate natural non-rotating freqs
oTN=[0.5 1.5 2.5]*pi*sqrt(GJ/(Ia*R^2));
oR=sqrt(oN.*oN+(K0+K1*e).*O^2);            % Calculate natural rotating freqs
oTR=(O.^2+oTN.^2).^(1/2);
W=[Gmass; oN; oR]'                         % Display bending results
X=[GTmass; oTN; oTR]'                      % Display torsion results

Vfwd=linspace(mn,mx,300)*12;               % Set range of airspeeds for helicopter
ktip=b*oTR(1)./(Vfwd+O*R);                 % Define reduced frequency for tip

for q=1:length(ktip)                       % validate Theodorsen calculations
   H1(q)=besselh(1,2,ktip(q));             % by comparing w/ F and -G plots
   H0(q)=besselh(0,2,ktip(q));             % from prior works
   C(q)=H1(q)/(H1(q)+i*H0(q));
   RE(q)=real(C(q));
   IM(q)=imag(C(q));
end
figure(2)        % Plot Theodorsen lift deficiency function for our range
semilogx(ktip,RE,ktip,-IM)
legend('F','-G');

for n=1:3                          % Calculate static moments for mode coupling
   for m=1:2
      Sa(n,m)=sum(Salf*f(:,n).*F(:,m));
   end
end

pirho=pi*rho;
oa1=oTR(1);
for q=1:length(Vfwd)               % Run entire blade for range of values k at blade tip
   for t=1:length(mid)             % Calc Theodorsen coeff's for each element of blade
      K(t)=(b*oa1)./(Vfwd(q)+(O*R*mid(p+1-t)));
      H1(t)=besselh(1,2,K(t));
      H0(t)=besselh(0,2,K(t));
      C(t)=H1(t)/(H1(t)+i*H0(t));                    % Theodorsen's function
      Lh(t)=(1-2*i*C(t)/K(t));                       % Lift - plunge
      La(t)=(0.5-2*i*(0.5+(1-i/K(t))*C(t))/K(t));    % Lift - pitch
      Mh(t)=(0.5);                                   % Moment - plunge
      Ma(t)=(3/8-i/K(t));                            % Moment - pitch
   end
```

```
% % % % % Calculate A matrix (Generalized Force Matrix)
   A(1,1)=sum(d*Lh(:)*b^2.*f(:,1).^2);                          % in^3
   A(1,2)=sum(d*Lh(:)*b^2.*f(:,1).*f(:,2));                     % in^3
   A(1,3)=sum(d*Lh(:)*b^2.*f(:,1).*f(:,3));                     % in^3
   A(1,4)=sum(d*(La(:)-(0.5+a)*Lh(:))*b^3.*f(:,1).*F(:,1));     % in^4
   A(1,5)=sum(d*(La(:)-(0.5+a)*Lh(:))*b^3.*f(:,1).*F(:,2));     % in^4
   A(2,1)=A(1,2);                                               % in^3
   A(2,2)=sum(d*Lh(:)*b^2.*f(:,2).^2);                          % in^3
   A(2,3)=sum(d*Lh(:)*b^2.*f(:,3).*f(:,2));                     % in^3
   A(2,4)=sum(d*(La(:)-(0.5+a)*Lh(:))*b^3.*f(:,2).*F(:,1));     % in^4
   A(2,5)=sum(d*(La(:)-(0.5+a)*Lh(:))*b^3.*f(:,2).*F(:,2));     % in^4
   A(3,1)=A(1,3); A(3,2)=A(2,3);                                % in^3
   A(3,3)=sum(d*Lh(:)*b^2.*f(:,3).^2);                          % in^3
   A(3,4)=sum(d*(La(:)-(0.5+a)*Lh(:))*b^3.*f(:,3).*F(:,1));     % in^4
   A(3,5)=sum(d*(La(:)-(0.5+a)*Lh(:))*b^3.*f(:,3).*F(:,2));     % in^4
   A(4,1)=sum(d*(Mh(:)-(0.5+a)*Lh(:))*b^3.*f(:,1).*F(:,1));     % in^4
   A(4,2)=sum(d*(Mh(:)-(0.5+a)*Lh(:))*b^3.*f(:,2).*F(:,1));     % in^4
   A(4,3)=sum(d*(Mh(:)-(0.5+a)*Lh(:))*b^3.*f(:,3).*F(:,1));     % in^4
   A(4,4)=sum(d*(Ma(:)-(0.5+a)*(La(:)+Mh(:))+(0.5+a)^2*Lh(:))
              *b^4.*F(:,1).^2);                                 % in^5
   A(4,5)=sum(d*(Ma(:)-(0.5+a)*(La(:)+Mh(:))+(0.5+a)^2*Lh(:))
              *b^4.*F(:,1).*F(:,2));                            % in^5
   A(5,1)=sum(d*(Mh(:)-(0.5+a)*Lh(:))*b^3.*f(:,1).*F(:,2));     % in^4
   A(5,2)=sum(d*(Mh(:)-(0.5+a)*Lh(:))*b^3.*f(:,2).*F(:,2));     % in^4
   A(5,3)=sum(d*(Mh(:)-(0.5+a)*Lh(:))*b^3.*f(:,2).*F(:,2));     % in^4
   A(5,4)=A(4,5);                                               % in^5
   A(5,5)=sum(d*(Ma(:)-(0.5+a)*(La(:)+Mh(:))+(0.5+a)^2*Lh(:))
              *b^4.*F(:,2).^2);                                 % in^5

% % % % % Incorporate pi, rho, generalized masses and MOI correction
   Adim(1,1)=pirho*A(1,1)+Gmass(1);                             % lbs^2/in
   Adim(1,2)=pirho*A(1,2);                                      % lbs^2/in
   Adim(1,3)=pirho*A(1,3);                                      % lbs^2/in
   Adim(1,4)=pirho*A(1,4)+Sa(1,1);                              % lbs^2
   Adim(1,5)=pirho*A(1,5)+Sa(1,2);                              % lbs^2
   Adim(2,1)=pirho*A(2,1);                                      % lbs^2/in
   Adim(2,2)=pirho*A(2,2)+Gmass(2);                             % lbs^2/in
   Adim(2,3)=pirho*A(2,3);                                      % lbs^2/in
   Adim(2,4)=pirho*A(2,4)+Sa(2,1);                              % lbs^2
   Adim(2,5)=pirho*A(2,5)+Sa(2,2);                              % lbs^2
   Adim(3,1)=pirho*A(3,1);                                      % lbs^2/in
   Adim(3,2)=pirho*A(3,2);                                      % lbs^2/in
   Adim(3,3)=pirho*A(3,3)+Gmass(3);                             % lbs^2/in
   Adim(3,4)=pirho*A(3,4)+Sa(3,1);                              % lbs^2
   Adim(3,5)=pirho*A(3,5)+Sa(3,2);                              % lbs^2
   Adim(4,1)=pirho*A(4,1)+Sa(1,1);                              % lbs^2
```

```
   Adim(4,2)=pirho*A(4,2)+Sa(2,1);                  % lbs^2
   Adim(4,3)=pirho*A(4,3)+Sa(3,1);                  % lbs^2
   Adim(4,4)=pirho*A(4,4)+GTmass(1);                % lbins^2
   Adim(4,5)=pirho*A(4,5);                          % lbins^2
   Adim(5,1)=pirho*A(5,1)+Sa(1,2);                  % lbs^2
   Adim(5,2)=pirho*A(5,2)+Sa(2,2);                  % lbs^2
   Adim(5,3)=pirho*A(5,3)+Sa(3,2);                  % lbs^2
   Adim(5,4)=pirho*A(5,4);                          % lbins^2
   Adim(5,5)=pirho*A(5,5)+GTmass(2);                % lbins^2

% % % % % Manipulate A matrix to be eigenvalue friendly
   Abar(1,1)=(Adim(1,1)/Gmass(1))*(oTR(1)/oR(1))^2;
   Abar(1,2)=(Adim(1,2)/Gmass(1))*(oTR(1)/oR(1))^2;
   Abar(1,3)=(Adim(1,3)/Gmass(1))*(oTR(1)/oR(1))^2;
   Abar(1,4)=(Adim(1,4)/Gmass(1))*(oTR(1)/oR(1))^2;     % in
   Abar(1,5)=(Adim(1,5)/Gmass(1))*(oTR(1)/oR(1))^2;     % in
   Abar(2,1)=(Adim(2,1)/Gmass(2))*(oTR(1)/oR(2))^2;
   Abar(2,2)=(Adim(2,2)/Gmass(2))*(oTR(1)/oR(2))^2;
   Abar(2,3)=(Adim(2,3)/Gmass(2))*(oTR(1)/oR(2))^2;
   Abar(2,4)=(Adim(2,4)/Gmass(2))*(oTR(1)/oR(2))^2;     % in
   Abar(2,5)=(Adim(2,5)/Gmass(2))*(oTR(1)/oR(2))^2;     % in
   Abar(3,1)=(Adim(3,1)/Gmass(3))*(oTR(1)/oR(3))^2;
   Abar(3,2)=(Adim(3,2)/Gmass(3))*(oTR(1)/oR(3))^2;
   Abar(3,3)=(Adim(3,3)/Gmass(3))*(oTR(1)/oR(3))^2;
   Abar(3,4)=(Adim(3,4)/Gmass(3))*(oTR(1)/oR(3))^2;     % in
   Abar(3,5)=(Adim(3,5)/Gmass(3))*(oTR(1)/oR(3))^2;     % in
   Abar(4,1)=Adim(4,1)/GTmass(1);                       % /in
   Abar(4,2)=Adim(4,2)/GTmass(1);                       % /in
   Abar(4,3)=Adim(4,3)/GTmass(1);                       % /in
   Abar(4,4)=Adim(4,4)/GTmass(1);
   Abar(4,5)=Adim(4,5)/GTmass(1);
   Abar(5,1)=(Adim(5,1)/GTmass(2))*(oTR(1)/oTR(2))^2; % /in
   Abar(5,2)=(Adim(5,2)/GTmass(2))*(oTR(1)/oTR(2))^2; % /in
   Abar(5,3)=(Adim(5,3)/GTmass(2))*(oTR(1)/oTR(2))^2; % /in
   Abar(5,4)=(Adim(5,4)/GTmass(2))*(oTR(1)/oTR(2))^2;
   Abar(5,5)=(Adim(5,5)/GTmass(2))*(oTR(1)/oTR(2))^2;

% Define Matrix for 3 or 5 mode analysis
   if mode==3
      T(1,1)=Abar(1,1); T(1,2)=Abar(1,2); T(1,3)=Abar(1,4);
      T(2,1)=Abar(2,1); T(2,2)=Abar(2,2); T(2,3)=Abar(2,4);
      T(3,1)=Abar(4,1); T(3,2)=Abar(4,2); T(3,3)=Abar(4,4);
   else
      T=Abar;
   end
```

```
   Z(:,q)=eig(T,'nobalance');          % Calculate eigenvalues w/o conditioning
   [Zz(:,q),index]=sort(real(Z(:,q))); % sort by real part (frequency part)
   Z1(:,q)=Z(index,q);                 % must keep real & imag parts together
   ZR(:,q)=real(Z1(:,q));
   ZI(:,q)=imag(Z1(:,q));
   o(:,q)=real(oTR(1)./sqrt(ZR(:,q)));
                % the assumption of real frequencies is implicit p.340 S&R
   g(:,q)=ZI(:,q)./ZR(:,q);            % damping matrix
end

% Generate x-axis values for plotting
% Only need to calculate values for the unstable mode
% Since only the flutter point is a true representation of reality
x=1./ktip;
if mode==3
   V2=(o(2,q)*b/12).*x; % velocity corresponding to actual oTR(1) in fwd flight
else
   V2=(o(4,q)*b/12).*x; % velocity corresponding to actual oTR(1) in fwd flight
end

% Save output file for incorporation into spreadsheet program (better plotting)
spread=[g; o; V2]';
dlmwrite('APlot100.txt',spread,'\t',1,1);
% Display graphs of mode freqs & damping coeff's versus tip velocity and 1/Ktip
figure(3);
subplot(2,1,1)
plot(V2,g)
axis([700,1100,-0.5,0.1])
grid on
xlabel('Tip Velocity (ft/s)'); ylabel('damping coefficient');
subplot(2,1,2)
plot(V2,o)
axis([700,1100,50,150])
grid on
xlabel('Tip Velocity (ft/s)'); ylabel('frequency of oscillation');
figure(4)
subplot(2,1,1)
semilogx(x,g)
grid on
xlabel('1 / Ktip'); ylabel('damping coefficient');
axis([min(x),max(x),-0.5,0.1])
subplot(2,1,2)
semilogx(x,o)
grid on
xlabel('1 / Ktip'); ylabel('frequency of oscillation');
axis([min(x),max(x),50,150])
```

LIST OF REFERENCES

1. Wood, E. R., Couch, Mark A., and Canright, D., "On the Flutter Speed of a Rotor Blade in Forward Flight", 28th European Rotorcraft Forum, Bristol, England, 2002.

2. Loewy, R. G., "A Two-Dimensional Approach to the Unsteady Aerodynamics of Rotary Wings," Journal of the Aeronautical Sciences, Vol. 24, Feb. 1957, pp. 82-98.

3. Jones, W. P. and Rao, B. M., "Compressibility Effects on Oscillating Rotor Blades in Hovering Flight," Volume of Technical Papers on Structural Dynamics and Aeroelasticity Specialist Conference, New Orleans, LA, April 16-17, 1969.

4. Hammond, C.E., "Compressibility Effects in Helicopter Rotor Blade Flutter," Ph.D. thesis, Dec. 1969, Georgia Institute of Technology.

5. Shipman, K. W. and Wood, E. R., "A Two-Dimensional Theory for Rotor Blade Flutter in Forward Flight," AIAA Journal of Aircraft, Vol. 8, No. 12, pp. 1008-1015, December 1971.

6. Wood, E. R., Vibration and Flutter Report 50131 for Advanced Tactical Helicopter, Sikorsky Aircraft, Stratford, Connecticut, 1960.

7. Theodorsen, T., "General Theory of Aerodynamic Instability and the Mechanism of Flutter," NACA Report. 496, 1935.

8. Scanlan, R. H., and Rosenbaum, R., *Introduction to the Study of Aircraft Vibration and Flutter*, The Macmillan Co., New York, 1951.

9. Leishman, J. G., *Principles of Helicopter Aerodynamics*, Cambridge University Press, New York, 2000.

10. Jones, W.P., "Aerodynamic Forces on Wings in Non-uniform Motion," *Reports And Memo. 2117*, British Aeronautical Research Council, 1945.

11. Young, D. and Felgar, R. P., Jr., "Tables of Characteristic Functions Representing Normal Modes of Vibration of a Beam", Bulletin No. 4913, Bureau of Engineering Research, The University of Texas, July, 1949.

12. Hartog, J. P. Den, *Mechanical Vibrations*, Dover Publications, New York, 1985.

13. Yntema, R. T., "Simplified Procedures and Charts for the Rapid Estimation of Bending Frequencies of Rotating Beams", NACA Technical Note 3459, Langley Field, VA, June 1955.

14. Bramwell, A.R.S., *Helicopter Dynamics*, pp.290-326, Edward Arnold Publishers Ltd, 1976.

15. Yeo, H., Spreadsheet of Full-Scale, UH-60A Rotor Blade Structural Properties, Army/NASA Rotorcraft Division, Moffett Field, California, 2001 (unpublished).

INITIAL DISTRIBUTION LIST

1. Defense Technical Information Center
   Ft. Belvoir, Virginia

2. Dudley Knox Library
   Naval Postgraduate School
   Monterey, California

3. Dr. E. R. Wood
   Naval Postgraduate School
   Monterey, California

4. CDR Mark A. Couch
   Naval Postgraduate School
   Monterey, California

5. Dr. Max Platzer
   Naval Postgraduate School
   Monterey, California